

1 **Endothelial Unc5B controls blood-brain barrier integrity**

2
3 Kevin Boyé¹, Luiz Henrique Geraldo^{1,2}, Jessica Furtado¹, Laurence Pibouin-Fragner²,
4 Mathilde Poulet^{1,2}, Doyeun Kim³, Bryce Nelson⁴, Yunling Xu², Laurent Jacob², Nawal
5 Maissa², Bertrand Tavitian², Dritan Agalliu⁵, Lena Claesson-Welsh⁶, Susan L Ackerman⁷,
6 Anne Eichmann^{1,2,8#}

7
8
9 1 Cardiovascular Research Center, Department of Internal Medicine, Yale University
10 School of Medicine, New Haven CT, USA.

11 2 Paris Cardiovascular Research Center, Inserm U970, Université Paris, France.

12 3 Medicinal Bioconvergence Research Center, Yonsei University, Incheon, Republic of
13 Korea

14 4 Department of Pharmacology, Cancer Biology Institute, Yale University School of
15 Medicine, New Haven, CT, USA.

16 5 Departments of Neurology and Pathology and Cell Biology, Columbia University Irving
17 Medical Center, New York NY, USA.

18 6 Department of Immunology, Genetics and Pathology, Uppsala University, Uppsala,
19 Sweden.

20 7 Division of Biological Sciences Section of Neurobiology and Department of Cellular and
21 Molecular Medicine, University of California San Diego and Howard Hughes Medical
22 Institute, La Jolla CA, USA.

23 8 Department of Molecular and Cellular Physiology, Yale University School of Medicine,
24 New Haven CT, USA.

25 # author for correspondence

26 **Abstract**

27

28 Blood-brain barrier (BBB) integrity is critical for proper function of the central
29 nervous system (CNS). Here, we showed that the endothelial Netrin1 receptor Unc5B
30 controls BBB integrity by maintaining Wnt/β–catenin signaling. Inducible endothelial-
31 specific deletion of Unc5B in adult mice led to region and size-selective BBB opening.
32 Loss of Unc5B decreased BBB Wnt/β–catenin signaling, and β–catenin overexpression
33 rescued *Unc5B* mutant BBB defects. Mechanistically, Netrin1 enhanced Unc5B
34 interaction with the Wnt co-receptor LRP6, induced its phosphorylation and activated
35 Wnt/β–catenin downstream signaling. Intravenous delivery of antibodies blocking Netrin1
36 binding to Unc5B caused a transient disruption of Wnt signaling and BBB breakdown,
37 followed by neurovascular barrier resealing. These data identify Netrin-Unc5B signaling
38 as a novel regulator of BBB integrity with potential therapeutic utility for CNS diseases.

39

40 **Introduction**

41
42 The BBB protects the brain from toxins and pathogens and maintains homeostasis
43 and proper function of the CNS^{1,2}. Wnt/β-catenin signaling maintains BBB integrity via
44 expression of either Wnt7a,7b or Norrin ligands, which bind to multiprotein receptor
45 complexes including Frizzled4 and LRP6 on brain endothelial cells (ECs) in distinct CNS
46 regions³⁻⁵. Receptor activation causes β-catenin stabilization and nuclear translocation
47 to induce expression of a BBB-specific gene transcription repertoire, including the tight
48 junction (TJ)-associated protein Claudin5 that suppresses paracellular permeability, while
49 inhibiting expression of the permeability protein PLVAP that forms the diaphragm in EC
50 fenestrae and transcytotic vesicles⁶⁻⁹. Whether Wnt/β-catenin signaling could be
51 modulated to open the BBB “on-demand” or to restore its integrity when damaged, is
52 unknown.

53 Here, we have identified the endothelial Unc5B receptor and its ligand Netrin1 as
54 novel regulators of Wnt/β-catenin signaling at the BBB. Unc5B is a transmembrane
55 receptor for Netrin1^{10,11}, Robo4^{12,13} and Flrt2^{14,15} that is predominantly expressed in ECs
56 in mice and humans¹⁶. Global *Unc5B* knockout in mice is embryonically lethal due to
57 vascular defects^{14,16}, demonstrating that Unc5B has important functions in vascular
58 development. Whether Unc5B signaling is required in postnatal mice or in adults
59 remained unknown.

60

61 **Results**

62 *Unc5B controls BBB development and maintenance.*

63 We generated tamoxifen (TAM)-inducible, endothelial-specific *Unc5B* knockout
64 mice by crossing *Unc5B*^{fl/fl} mice (**Supp. Fig. 1a**) with *Cdh5CreERT2* mice¹⁷ (hereafter
65 Unc5BiECko), which deletes in ECs. Gene deletion was induced by TAM injection in
66 neonates between postnatal day (P)0-P2, and qPCR revealed efficient *Unc5B* deletion
67 (**Supp. Fig. 1b,c**). Interestingly, neonatal TAM injection induced seizures and lethality of
68 Unc5BiECko mice around P15 (**Supp. Fig. 1d, Supp videos 1-4**), indicating an abnormal
69 excitability of the neuronal network that may result from a BBB failure². Intraperitoneal
70 injection of a fluorescent tracer cadaverine (MW 950Da) into P5 mice and analysis of

71 tracer leak 2hrs later revealed widespread tracer extravasation into the brain of P5
72 Unc5BiECko mice, which confirmed that Unc5B deletion impaired BBB development
73 (**Supp. Fig. 1,e**).

74 To determine if Unc5B also controlled BBB integrity in adults, we induced gene
75 deletion and probed BBB integrity 7 days later by intravenous (i.v.) injection of fluorescent
76 tracers (**Fig.1a**). Cadaverine remained inside the vasculature of TAM injected Cre-
77 littermate controls but leaked into the Unc5BiECko brain (**Fig. 1b**). Cadaverine leakage
78 was observed in several regions of adult Unc5BiECko brains, including the retrosplenial
79 and piriform cortex, hippocampus, hypothalamus, thalamus, striatum and cerebellum,
80 while other cortical areas such as the posterior parietal association areas and the primary
81 somatosensory cortex displayed an intact BBB (**Fig. 1c**). Injection of fluorescent dextrans
82 of increasing molecular weights showed that both 10kDa and 40kDa dextrans had a
83 higher permeability across the BBB in Unc5BiECko brains compared to controls, whereas
84 70kDa dextran did not cross the BBB, suggesting a size selective defect of BBB leakage
85 for proteins greater than 40kDa in Unc5BiECko mice (**Fig. 1d**). The vascular permeability
86 to cadaverine and 40kDa dextran in other Unc5BiECko organs was similar to controls
87 (**Supp. Fig.1f**), demonstrating that Unc5B has a CNS-selective BBB protective function
88 in adult mice, which may be due to its enriched expression in adult brain endothelium
89 when compared to endothelium of other organs¹⁸.

90 Staining of adult brain sections with a commercial antibody recognizing Unc5B
91 showed labeling of endothelium in various brain regions (**Supp. Fig. 2a**) and revealed
92 that Unc5B deletion had no effect on vascular density (**Fig. 1e,f**). Unc5B expression was
93 also detected in a few CD13⁺ pericytes (**Supp. Fig. 2b**). Because pericytes contribute to
94 BBB integrity^{19,20}, we determined whether pericyte-derived Unc5B affected the BBB by
95 crossing the *Unc5B*^{fl/fl} mice with *PdgfrβCre*^{ERT2} mice²¹ (Unc5BiPCko), to delete *Unc5B* in
96 mural cells. Neither TAM-treated Cre-negative littermate controls, nor Unc5BiPCko mice
97 showed cadaverine leakage across the BBB (**Fig. 1g,h**). Hence, endothelial, but not
98 pericyte, Unc5B controls adult BBB integrity.

99
100
101

102 *Unc5B regulates Wnt/β-catenin signaling.*

103 To determine the cause of the BBB defect, we measured expression levels of
104 Claudin5 and PLVAP as well as markers for pericytes and astrocytes^{19,20,22-24}. Compared
105 to TAM-treated Cre-negative littermate controls, Unc5BiECko mice showed significantly
106 reduced expression of Claudin5, along with increased expression of PLVAP (**Fig.1 i,j**).
107 By contrast, western blot and immunostaining showed that expression of other BBB
108 regulators such as Caveolin1 (in ECs), PDGFRβ (in pericytes), GFAP and Aquaporin-4
109 (in astrocytes) were similar between genotypes (**Supp. Fig. 3 a-d**).

110 Homozygous global *Unc5B* KO E12.5 embryos¹⁶ exhibited decreased Claudin5
111 and increased PLVAP expressions in the brain (**Supp. Fig. 3e-g**), validating *Unc5B*
112 deletion effects on Claudin5 and PLVAP in an independent knockout mouse strain.
113 Immunolabeling of adult brain sections showed decreased Claudin5 and increased
114 PLVAP expression in areas with cadaverine leakage in Unc5BiECko brains (**Fig. 1k**),
115 suggesting that BBB leakage may be due to changes in expression of Claudin5 and
116 PLVAP.

117 Because Claudin5 and PLVAP are two known targets of Wnt/β-catenin signaling⁶⁻
118 ⁹, we determined if Unc5B affected Wnt signaling at the BBB. Western-blot analysis on
119 brain lysates revealed a significant decrease of β-catenin and the LEF1 transcriptional
120 effector in Unc5BiECko brains compared to littermate controls (**Fig. 2a-b**), and
121 immunostaining confirmed decreased LEF1 expression in brain ECs of Unc5BiECko mice
122 (**Fig. 2c-d**). Moreover, phosphorylation of LRP6 at S1490, a hallmark of Wnt/β-catenin
123 pathway activation, was dramatically downregulated upon *Unc5B* gene deletion (**Fig. 2a-**
124 **b**). This phosphorylation provides a docking site for the adapter protein Axin1, resulting
125 in inhibition of the β-catenin destruction complex and thereby promoting β-catenin
126 nuclear translocation and activation^{25,26}.

127 Immunoprecipitation of Unc5B from primary microvascular mouse brain ECs
128 pulled down LRP6 (**Fig. 2e**), demonstrating a physical interaction between Unc5B and
129 LRP6 receptors. To determine which Unc5B domain mediated this interaction, we
130 infected Unc5B siRNA-treated human ECs with GFP-tagged siRNA resistant rat
131 adenoviral constructs encoding Unc5B full-length (FL) or a cytoplasmic domain deletion

132 (ΔCD) (**Fig. 2f**). LRP6 co-IP was rescued by Unc5B FL but not by ΔCD, identifying the
133 Unc5B cytoplasmic domain as the main LRP6 interacting domain. Additional cytoplasmic
134 domain deletions revealed that the Unc5B death domain (DD) that mediates apoptosis in
135 the absence of the ligand^{27,28} was dispensable for LRP6 interaction, whereas deletion of
136 the UPA domain (named after its conservation in Unc5B, PIDD and Ankyrin²⁸) abolished
137 LRP6 co-IP. Finally, a construct encoding only the cytoplasmic UPA domain was sufficient
138 to rescue LRP6 co-IP (**Fig. 2f-h**). Hence, Unc5B interacts with LRP6 via its UPA domain.

139 To test genetic interaction of Unc5B with Wnt/β–catenin signaling, we crossed
140 Unc5BiECko mice with *Ctnnb1*^{fl/fl} mice²⁹. Heterozygous Unc5B or β–catenin mice
141 displayed no BBB cadaverine leakage, but double heterozygous Unc5B^{fl/wt}; βcatenin^{fl/wt}–
142 *Cdh5Cre*^{ERT2} exhibited BBB cadaverine leakage compared to TAM treated Cre- controls
143 (**Fig. 2i,j**), demonstrating that Unc5B and β–catenin genetically interact to maintain BBB
144 integrity.

145 Next, we crossed Unc5BiECko with mice overexpressing an activated form of
146 β–catenin (*Ctnnb1*^{flex/3} mice) (**Fig. 2k**), which enhances Wnt/β–catenin signaling³⁰. The
147 resulting offspring (Unc5BiECko; *Ctnnb1*^{flex/3}) displayed decreased PLVAP protein
148 expression, along with increased LEF1 and Claudin5 protein expression compared to
149 Unc5BiECko mice (**Fig. 2l,m**). Cadaverine injection into Unc5BiECko; *Ctnnb1*^{flex/3} mice
150 showed that BBB leakage was reduced by β–catenin overexpression in Unc5BiECko
151 mice (**Fig. 2n**).

152 We considered other signaling pathways that could contribute to BBB leakage in
153 Unc5BiECko mice. Unc5B inhibits Vegfr2-mediated permeability signaling in ECs *in vitro*
154 by reducing phosphorylation of the Y949 residue¹³. Y949 phosphorylation is known to
155 trigger disassembly of adherens junctions by activating VE-Cadherin phosphorylation,
156 which then downregulates Claudin5^{12,13,31}. Therefore, increased brain Vegfr2-Y949
157 permeability signaling in the absence of Unc5B could contribute to BBB opening. Western
158 blotting of brain lysates revealed increased Vegfr2-Y949 phosphorylation in Unc5BiECko
159 compared to Cre- littermate controls, while Vegfr2-Y1173 phosphorylation, which is
160 critical for VEGF-induced proliferation, was unaffected (**Supp. Fig. 4a,b**). To test Vegfr2-
161 Y949 function, we crossed Unc5BiECko mice with Vegfr2-Y949F mutant mice, which
162 carry an inactivating substitution of tyrosine to phenylalanine and are resistant to VEGF-

163 induced permeability³². Injection of fluorescent cadaverine revealed increased dye
164 leakage into the brain of Unc5BiECko; Y949F mice compared to Cre- littermate controls
165 (**Supp. Fig. 4c,d**), demonstrating that Vegfr2-Y949F failed to rescue BBB integrity in
166 Unc5B mutant mice.

167 To discriminate between transcellular and paracellular vascular leakage in
168 Unc5BiECko mice, we crossed Unc5BiECko mice with eGFP::Claudin5 mice that express
169 2-fold higher Claudin5 levels compared to wildtype littermates³³ and thereby display
170 enhanced paracellular barrier properties of CNS ECs. BBB leakage of Cadaverine into
171 the brains of Unc5BiECko; eGFP::Claudin5 mice was reduced compared to Unc5BiECko
172 mice (**Supp. Fig. 4e,f**), demonstrating that Unc5B may regulate BBB leakage by
173 modulating the levels of Claudin5. However, leakage of 40kDa dextran remained
174 increased in Unc5BiECko; eGFP::Claudin5 mice compared to Unc5BiECko mice (**Supp.**
175 **Fig. 4g**), suggesting that loss of Unc5B induced both paracellular leak for small MW
176 tracers mediated by loss of Claudin5 as well as transcellular leak for higher MW dyes
177 potentially by inducing PLVAP.

178

179 *Netrin1 binding to Unc5B mediates BBB integrity.*

180 We then investigated whether Unc5B ligands Netrin1 and Robo4 regulated the
181 Wnt/β-catenin pathway activation in CNS ECs. Since Netrin1 mRNA is produced by
182 several cell types in the adult brain³⁴, we generated temporally inducible *Netrin1* global
183 KO mice by crossing *Ntn1^{fl/fl}* mice with *RosaCre^{ERT2}* mice (hereafter Ntn1iko), to induce
184 ubiquitous gene deletion upon TAM injection. Compared to TAM-treated Cre- littermate
185 controls, i.v. injection of cadaverine in adult Ntn1iko mice revealed increased cadaverine
186 leakage across the BBB (**Fig. 3a**), while *Robo4* KO mice¹² did not exhibit any BBB deficits
187 (**Fig. 3b**). Further analysis of adult Ntn1iko mouse brain lysates revealed efficient *Ntn1*
188 gene deletion along with decreased pLRP6, Claudin5 and LEF1 protein expression, while
189 PLVAP expression was increased (**Fig. 3c,d**). Moreover, treating serum-starved mouse
190 brain primary ECs with Netrin1 increased LRP6 phosphorylation with a peak at 30min to
191 8h after stimulation (**Fig. 3e,f**). This effect was abolished by *Unc5B* siRNA treatment
192 (**Fig. 3e,f**). Unc5B immunoprecipitation from mouse brain lysates revealed reduced LRP6
193 co-IP in the Ntn1iko mice when compared to controls (**Fig. 3g,h**), suggesting that Netrin1

194 binding to Unc5B regulated LRP6 phosphorylation and Wnt/β-catenin activation in CNS
195 ECs.

196 To specifically interrogate whether blocking Netrin1-Unc5B interactions disrupted
197 the BBB *in vivo*, we used monoclonal antibodies (mAbs) that we had previously generated
198 against the Unc5B IgG-like domains¹². Anti-Unc5B-1 recognizes human but not mouse
199 Unc5B, while anti-Unc5B-2 recognizes both human and mouse Unc5B and internalizes
200 Unc5B¹². Anti-Unc5B-2 treatment induced Unc5B internalization in brain ECs *in vitro*
201 (**Supp. Fig. 5a**) and i.v. injection of Anti-Unc5B-2 for 1 hour at 10mg/kg in mice reduced
202 brain Unc5B expression compared to anti-Unc5B-1 CTRL Ab-treated animals (**Supp. Fig.**
203 **5b,c**), therefore preventing binding of all Unc5B ligands *in vivo*.

204 To generate a mAb that specifically blocked Netrin1 binding without Unc5B
205 internalization, we screened a human phage-derived library against the entire rat Unc5B
206 extracellular domain and identified anti-Unc5B-3, a mAb that bound both human and
207 mouse Unc5B with high affinity (**Supp. Fig. 5d-f**) but did not induce Unc5B internalization
208 nor its degradation *in vivo* (**Supp. Fig. 5g,i**). I.v. injection of anti-Unc5B-3 for 15min at
209 10mg/kg followed by cardiac perfusion and immunolabelling using an anti-human IgG
210 antibody revealed anti-Unc5B-3 binding to the brain vasculature of *Unc5B^{fl/fl}*, but no
211 binding in the *Unc5BiECko* mice (**Supp. Fig. 5j,k**), demonstrating specific binding of anti-
212 Unc5B-3 to endothelial Unc5B. I.v. injection of anti-Unc5B-3 (10mg/kg for 1h) followed by
213 Unc5B immunoprecipitation revealed that anti-Unc5B-3 blocked Netrin1 binding to Unc5B
214 *in vivo* compared to CTRL Ab treated mice, while Robo4 and Flrt2 could still interact with
215 Unc5B (**Fig. 3i,j**). Anti-Unc5B-3 also blocked Netrin1-induced Src phosphorylation in
216 brain ECs *in vitro* (**Fig. 3k,l**).

217

218 *Transient ‘on demand’ BBB opening via anti-Unc5B antibodies.*

219 To test if antibody mediated Unc5B blockade could be used to open the BBB “on-
220 demand”, we injected i.v. CTRL or anti-Unc5B antibodies for 1hr in adult WT C57BL/6J
221 mice, followed by i.v. injection of fluorescent tracers of various molecular weights 30min
222 before sacrifice and analysis (**Fig. 3m**). In mice treated with CTRL Ab, there were no
223 signs of BBB disruption and injected cadaverine remained confined inside brain vessels
224 (**Fig. 3n,o**). In contrast, mice treated with anti-Unc5B-3 or anti-Unc5B-2 showed a

225 significant leakage of injected Cadaverine, 10kDa and 40kDa Dextran, but not 70kDa
226 Dextran or endogenous immunoglobulin or fibrinogen into the brain parenchyma (**Fig.**
227 **3n,o** and **Supp. Fig. 6a-c**), demonstrating that blocking Netrin1 binding to Unc5B is
228 sufficient to open the BBB. The vascular barrier disrupting effects of anti-Unc5B-2 and -3
229 were specific to the brain, as tracer leakage in other organs was similar between controls
230 and anti-Unc5B-2 or -3 treated mice (**Supp. Fig. 6d,e**).

231 Anti-Unc5B-3 treatment also enhanced delivery of single chain nanobodies
232 across the BBB when compared to CTRL Ab (**Fig.4a**), while nanobody extravasation in
233 other organs such as lung, heart, kidney or skin remained similar (**Supp. Fig. 6f**).
234 Moreover, injection of anti-Unc5B-3 mAbs enhanced brain delivery of BDNF and induced
235 phosphorylation and activation of its neuronal receptor Trk-B, while plasma BDNF levels
236 remained similar to CTRL Ab injected mice (**Fig.4b-d**), indicating that bioactive molecules
237 up to 40kDa can be delivered into the brain by this approach.

238 To determine the specific BBB vascular beds regulated by Unc5B, we injected
239 TAM in adult *BMXCre^{ERT2}-mTmG* mice that specifically express GFP in arteries upon
240 TAM injection, followed by anti-Unc5B-3 i.v. injection for 15 min and cardiac perfusion.
241 Human IgG staining of anti-Unc5B-3 revealed binding to GFP+ brain arteries at cell-cell
242 junctions but also to GFP- capillaries (**Supp. Fig.7a**), suggesting that Unc5B regulates
243 BBB integrity mainly in arteries and capillaries.

244 To assess anti-Unc5B bioavailability and vascular clearance, we injected anti-
245 Unc5B-3 antibodies (10mg/kg) i.v. for 1h, 8h or 24h followed by immune-labeling with
246 anti-human IgG antibodies (**Supp. Fig.7b**). Anti-Unc5B-3 was detectable in the brain
247 vasculature 1h after injection, declined to low levels after 8h and was undetectable 24h
248 after injection (**Supp. Fig.7b**), demonstrating rapid clearance from the brain vasculature.

249 Interestingly, the expression of Wnt/β-catenin downstream targets varied in a
250 similar time-dependent fashion. Claudin5 immunostaining was downregulated 1h after
251 anti-Unc5B-3 injection and returned to basal levels after 8h, whereas PLVAP
252 immunostaining was upregulated at 1 and 8h after anti-Unc5B-3 injection and returned to
253 low baseline levels after 24h (**Fig. 4e,f**). Western blot on brain protein lysates from mice
254 treated with CTRL Ab or anti-Unc5B-3 for 1h, 8h or 24h confirmed these changes (**Fig.**
255 **4g,h**). Unc5B immunoprecipitation showed that anti-Unc5B-3 treatment transiently

256 disrupted the Unc5B/LRP6 interaction 1h after anti-Unc5B-3 injection, thereby disrupting
257 Wnt/β–catenin signal transduction (**Fig. 4g,h**).

258 Finally, we provided a real time evidence of the transient opening of the BBB
259 mediated by anti-Unc5B treatment using both MRI and two-photon live imaging through
260 cranial windows. Mice received i.v. injection of CTRL or anti-Unc5B-2 mAb and were
261 imaged by contrast MRI after i.v. injection of gadoteric acid (MW 558 Da) at 1, 2, 3, 4 and
262 24 hours following antibody treatment. Quantification showed a significant gadoteric acid
263 leakage in the cortex and hippocampus between 1-4 hours after anti-Unc5B-2 delivery,
264 which returned to baseline levels after 24 hours (**Fig. 4i,j**), indicating that the
265 neurovascular barrier had resealed. Two-photon live imaging showed that a 2000kDa
266 FITC-dextran did not leak at any time point after anti-Unc5B-2 treatment but outlined the
267 brain vasculature (**Supp. Fig. 8a**). By contrast, Hoechst (MW 560Da) started to
268 extravasate from superficial cortical vessels within 5min after injection and continued to
269 leak over 30 minutes in mice that were treated with the anti-Unc5B-2 antibody one hour
270 prior to tracer injection (**Supp. Fig. 8a**). When 10kDa dextran was injected intravenously
271 in mice that were treated with the anti-Unc5B-2 antibody 24 hours earlier, we did not
272 observe any tracer leakage (**Supp. Fig. 8b**), indicating that the BBB had resealed.
273 However, re-administration of a second dose of anti-Unc5B-2 re-opened the BBB within
274 an hour leading to 10kDa dextran extravasation over the next 30 min (**Supp. Fig. 8b**).
275

276 **Discussion**

277 In summary, our data reveal Netrin1 signaling to Unc5B as a novel BBB regulatory
278 pathway with potential therapeutic relevance in CNS disease (**Supp. Fig. 9**). We showed
279 that mice deficient in either endothelial Unc5B receptor or Netrin1 ligand exhibited BBB
280 leakage accompanied by reduced expression of Wnt/β-catenin components, β-catenin
281 and LEF1. Moreover, i.v. delivery of Unc5B mAbs that specifically block Netrin1 binding
282 to Unc5B (anti-Unc5B-3), or that block binding of all Unc5B ligands via receptor
283 internalization (anti-Unc5B-2), led to transient Wnt/β-catenin signaling reduction and BBB
284 breakdown, supporting that Netrin1 binding to Unc5B is sufficient to maintain Wnt
285 signaling activation in CNS ECs and BBB integrity. Further experiments are required to
286 determine the source of Netrin1 mediating this effect. Single cell RNA sequencing studies

287 indicate that Netrin1 is highly expressed in adult brain pericytes, indicating that pericytes
288 are a likely source of Netrin1 production and Unc5B activation at the BBB³⁴. Interestingly,
289 Netrin1 was shown to be implicated in BBB integrity, upregulated in brain ECs in response
290 to brain injury, and to increase Claudin5 expression^{35,36}, therefore multiple cellular
291 sources and environmental modulations of Netrin1 expression could contribute to BBB
292 integrity. Since we could target Unc5B via i.v. blocking antibody injection, these data raise
293 the possibility that i.v. injection of Netrin1 or other Unc5B agonists could repair CNS
294 endothelial barrier breakdown in conditions such as ischemic stroke or multiple sclerosis
295 where the BBB is dysfunctional.

296 The BBB leakage in *Unc5B* mutants was region-specific and affected caudal and
297 ventral regions more than anterior and dorsal ones, which is roughly similar to the region-
298 specific BBB leakage observed in young adult mice carrying inducible allelic deletions of
299 β -catenin^{9,37}. The specific Wnt ligands and receptors that maintain the BBB differ in a
300 region-specific manner in the CNS, with cerebellum BBB utilizing Norrin, LRP5/6 and
301 TSPAN12 signaling module, while cortex relies on Wnt7a/b, GPR124, and RECK.
302 Ligands and receptors in different brain regions are partially redundant, in that inactivation
303 of several components exacerbates BBB leakage^{5,9,37}. Remarkably, blockade of Unc5B
304 function affected both the cortex, cerebellum and other brain regions, suggesting that
305 Unc5B may be an upstream regulator of several Wnt/Norrin signaling complexes at the
306 BBB. Mechanistically, we identify the Unc5B intracellular UPA domain as a regulator of
307 LRP6 interaction, suggesting that the UPA domain may induce LRP6 phosphorylation
308 through recruitment of kinases or other mechanisms that remain to be determined.
309 Recent studies in naïve pluripotent embryonic stem cells showed that Netrin1 binding to
310 Unc5B induced FAK-mediated phosphorylation of GSK3 α/β , a kinase implicated in LRP6
311 activation³⁸, suggesting one possible mechanism. Finally, because Unc5B is expressed
312 in arterial and capillary endothelium, but not in veins, it is likely to confer BBB integrity in
313 a vessel-segment specific manner, underscoring heterogeneity of BBB regulation in
314 different vascular segments³⁹.

315 Previous studies had speculated that transient Wnt signaling inhibition could be
316 used to open the BBB “on-demand” for drug delivery into the diseased CNS^{9,40}, but the
317 means to inhibit Wnt signaling in a CNS specific manner were not available. We

318 demonstrated that antibody mediated Unc5B blockade caused a transient loss of
319 Wnt/β-catenin signaling and BBB breakdown for 1h to 8h followed by neurovascular
320 barrier resealing, and allowed delivery of tracers up to 40kDa into the adult CNS. The size
321 selectivity of BBB opening is compatible with delivery of chemotherapeutics and of
322 bioactive molecules such as nanobodies and growth factors. Anti-Unc5B mAbs could
323 therefore synergize with existing therapies such as focused ultrasound/microbubble
324 approaches⁴¹⁻⁴⁴ and offer a new therapeutic perspective for treatment of various human
325 neurological disorders.

326

327 **Methods**

328 *Mouse models*

329 All protocols and experimental procedures were approved by the Institutional Animal Care
330 and Use Committee (IACUC). Generation of the targeted Unc5b allele was performed by
331 homologous recombination in R1 ES cells. Correctly targeted cells were identified by
332 Southern blot hybridization and injected into B6J blastocysts to generate Unc5bneo/+
333 mice. To remove the neo cassette, Unc5bneo/+ mice were mated to B6.129S4-
334 Gt(ROSA)26Sortm1(FLP1)Dym/RainJ mice (The Jackson Laboratory, stock #009086).
335 Mice were backcrossed to B6J mice for ten generations. Unc5B^{fl/fl} (B6-
336 Unc5b<tm1(flox)Slac/Slac) mice were then bred with Cdh5Cre^{ERT2} mice¹⁷ or
337 PDGFRβCre^{ERT2}²¹. eGFP::Claudin5 transgenic mice, Y949F mice, βcatenin GOF
338 Ctnnb1^{flex/3} mice, βcatenin^{fl/fl} mice, Robo4^{-/-} mice and Netrin1^{fl/fl} mice were described
339 previously^{12,29,30,32,33,45}. Gene deletion was induced by injection of tamoxifen (Sigma
340 T5648) diluted in corn oil (Sigma C8267). Postnatal gene deletion was induced by 3
341 injections of 100ug of tamoxifen at P0, P1 and P2; whereas adult gene deletion was
342 induced by 5 injections of 2mg of tamoxifen from P60 to P64.

343

344 *Cell culture*

345 Bend3 cells were purchased from ATCC (ATCC® CRL-2299™) and C57BL/6 Mouse
346 Primary Brain Microvascular Endothelial Cells were purchased from Cell Biologics (C57-
347 6023). Cells were cultured in Dulbecco's Modified Eagle's Medium (DMEM) high glucose

348 (Thermo Fisher Scientific, 11965092) supplemented with 10% fetal bovine serum (FBS)
349 and 1% Penicillin Streptomycin at 37 °C and 5% CO₂ and split when confluent using
350 Trypsin-EDTA (0.05%) (Life Technologies, 25300054). When indicated, cells were
351 stimulated using Recombinant Mouse Netrin-1 Protein (R&D, 1109-N1-025) at 500ng/ml.
352

353 *Western-Blot*

354 Brains were dissected and frozen in liquid nitrogen. They were lysed in RIPA buffer
355 (Research products, R26200-250.0) supplemented with protease and phosphatase
356 inhibitor cocktails (Roche, 11836170001 and 4906845001) using a Tissue-Lyser (5 times
357 5min at 30 shakes/second). For western blot on cell culture, cells were washed with PBS
358 and lysed in RIPA buffer with protease and phosphatase inhibitors cocktails. All protein
359 lysates were then centrifuged 15min at 13200RPM at 4°C and supernatants were
360 isolated. Protein concentration were quantified by BCA assay (Thermo Scientific, 23225)
361 according to the manufacturer's instructions. 30ug of protein were diluted in Laemmli
362 buffer (Bio-Rad, 1610747) boiled at 95°C for 5min and loaded in 4-15% acrylamide gels
363 (Bio-Rad, 5678084). After electrophoresis, proteins were transferred on a polyvinylidene
364 difluoride (PVDF) membrane and incubated in TBS 0.1% Tween supplemented with 5%
365 BSA for 1hour to block non-specific binding. The following antibodies were incubated
366 overnight at 4°C: Unc5B (Cell Signaling, 13851S), Robo4 (Invitrogen, 20221-1-AP), Flrt2
367 (Novus bio, NBP2-43653), Netrin1 (R&D, AF1109), Claudin5 (Invitrogen, 35-2500),
368 PLVAP (BD biosciences, 550563), PDGFR β (Cell Signaling, 3169S), GFAP (DAKO,
369 Z0334), VEGFR2 Y949 (Cell Signaling, 4991S), VEGFR2 Y1173 (Cell Signaling, 2478S),
370 pLRP6 (Cell Signaling, 2568S), LRP6 (Cell Signaling, 3395S), β catenin (Cell Signaling,
371 8480S), LEF1 (Cell Signaling, 2230S) and β actin (Sigma, A1978). Then, membranes
372 were washed 4 x 10min in TBS 0.1% Tween and incubated with one of the following
373 peroxidase-conjugated secondary antibodies diluted in TBS 0.1% Tween supplemented
374 with 5%BSA for 2h at room temperature: horse anti-mouse IgG(H+L) (Vector laboratories,
375 PI-2000), goat anti-rabbit IgG(H+L) (Vector laboratories, PI-1000), goat anti-rat IgG(H+L)
376 (Vector laboratories, PI-9400), horse anti-goat IgG(H+L) (Vector laboratories, PI-9500).
377 After 4 x 10min wash, western blot bands were acquired using ECL western blotting
378 system (Thermo Scientific, 32106) or west femto maximum sensitivity substrate (Thermo

379 Scientific, 34095) on a Biorad Gel Doc EQ System with Universal Hood II imaging system
380 equipped with Image Lab software.

381

382 *Immunoprecipitation*

383 Pierce™ protein A/G magnetic beads (Thermo fischer, 88802) were washed 5 times
384 10min with RIPA buffer. 300ug of protein lysate were diluted in 1ml of RIPA buffer
385 containing protease and phosphatase inhibitors and were incubated with 30ul of A/G
386 magnetic beads for 1hour at 4°C under gentle rotation. Protein lysates were harvested
387 using a magnetic separator (Invitrogen) and were incubated overnight at 4°C under gentle
388 rotation with 10ug of Unc5B antibody (R&D, AF1006) or control IgG. The next day, 40ul
389 of protein A/G magnetic beads were added to each protein lysate for 2hour at 4°C under
390 gentle rotation. Beads were then isolated using a magnetic separator and washed 5 x
391 with RIPA buffer. After the last wash, supernatants were removed and beads were
392 resuspended in 40ul of Laemmlli buffer (Bio-Rad, 1610747), boiled at 95°C for 5min and
393 loaded onto 4-15% gradient acrylamide gels. Western blotting was performed as
394 described above.

395

396 *Immunostaining*

397 Brains were collected and placed in 3.7% formaldehyde overnight at 4°C. Brains were
398 then washed 3 times 10min with TNT buffer (for 100ml: 10ml Tris 1M pH7,4, 3ml NaCl
399 5M, 500ul Triton X-100) and embedded in 2% agarose. 150um sections were prepared
400 using a Leica VT 1000S vibratome and placed in TNTB buffer (TNT buffer supplemented
401 with 5% donkey serum) for 24h at 4°C. Primary antibodies were diluted in TNTB and
402 placed for 48h at 4°C under gentle agitation. Then, sections were washed 5 times 30min
403 with TNT buffer and incubated for 24h at 4°C with secondary antibodies diluted in TNTB
404 buffer. After 5 x 30min wash with TNT, sections were mounted using DAKO mounting
405 medium (Agilent, S302380-2).

406 For brain endothelial cell immunostaining, cells were seeded on 18mm glass coverslips
407 (Fischer Scientific, 12542A). When confluent, cells were washed with PBS and fixed with
408 3.7% formaldehyde for 10min. Cells were washed 3 times 5min with PBS and were

409 incubated with 0.2% TritonX100 diluted in PBS for an additional 10min, washed 3 times
410 and incubated with blocking solution (2%BSA, 3%Donkey serum diluted in PBS) for 1hour
411 at room temperature. Primary antibodies were then diluted in blocking solution and
412 incubated on coverslips overnight at 4°C. After 3 x 5min washes, secondary antibodies
413 diluted in blocking buffer were incubated on coverslips for 2h at room temperature.
414 Coverslips were then washed 3 times 5min with PBS and mounted using DAKO mounting
415 medium.

416 The following antibodies were used: Podocalyxin (RD, AF1556), Unc5B (Cell signaling,
417 13851S), Claudin5-GFP (Invitrogen, 352588), GFAP (Millipore, MAB360), Aquaporin4
418 (Millipore, AB3068), PDGFR β (Cell Signaling, 3169S), LEF1 (Cell Signaling, 2230S),
419 Endomucin (Hycult biotech, HM1108), fibrinogen (DAKO, A0080), DAPI (Thermo Fischer,
420 62248). All corresponding secondary antibodies were purchased from Invitrogen as Alexa
421 Fluor (488, 568, 647) donkey anti-primary antibodies (H+L).

422

423 *Small interfering RNA knockdown experiments*

424 For Unc5B Inhibition, cells were transiently transfected with siRNA (Dharmacon). ON-
425 TARGETplus Mouse Unc5b siRNA (SMARTpool, L-050737-01-0005) were used for
426 Unc5B gene deletion. Transfection was performed using lipofectamine RNAi max
427 (Invitrogen, 13778-075) according to the manufacturer's instruction with siRNA at a final
428 concentration of 25pmol in OptiMem for 8h. After transfection, cells were washed with
429 PBS and fresh complete media was added for 48h.

430

431 *Mouse lung endothelial cell isolation*

432 Mouse lung were collected and minced into small pieces. Lungs were incubated in
433 digestion buffer (5ml of DMEM supplemented with 5mg of collagenase I (Worthington
434 LS004196), 10ul of 1M Ca $^{2+}$ and 10ul of 1M Mg $^{2+}$) for 1hour at 37°C with shaking every
435 10min. Once fully lysed, lung lysates were filtered through a 40um cell strainer (Falcon,
436 352340) into a solution of 3ml FBS. Samples were centrifuged for 10min at 1500RPM
437 and pellets were resuspended in PBS 0.1%BSA. In the meantime, rat anti-mouse CD31
438 (BD Pharmigen, 553370) was incubated with sheep anti-rat IgG magnetic dynabeads

439 (Invitrogen, 11035) in a solution of sterile PBS 0.1%BSA (120ul of beads, 24ul of
440 antibodies in 12ml PBS 0.1%BSA). Solutions were place under gentle rotation at room
441 temperature for 2hours to allow proper coupling of antibodies and beads. Coupled beads
442 were next isolated using a magnetic separator and incubated in the resuspended lung
443 lysate for 30min. After 5 washes with PBS 0.1%BSA, beads were separated using
444 magnetic separator and seeded in 60mm dishes containing mouse lung endothelial cell
445 media (DMEM high glucose, 20%FBS, 1% Penicillin Streptomycin, 2% mitogen (Alta
446 Aesar BT203). Purified endothelial cells were cultured at 37 °C and 5% CO2 until
447 confluence was reached, and then harvested.

448

449 *Quantitative real-time PCR analysis*

450 mRNA were isolated using Trizol reagent (Life Technologies, 15596018) according to the
451 manufacturer's instructions and quantified RNA concentrations using nanodrop 2000
452 (Thermo Scientific). 300ng of RNA were reverse transcribed into cDNA using iScript
453 cDNA synthesis kit (Bio-rad, 170-8891). Real-time qPCR was then performed in
454 duplicates using CFX-96 real time PCR device (Bio-rad). Mouse GAPDH (QT01658692)
455 was used as housekeeping gene for all reactions.

456

457 *Unc5B function blocking antibody generation*

458 We performed a Phage-Fab (antigen-binding fragment) selection using a naïve Fab
459 library (libF⁴⁶) on an immobilized recombinant rat Unc5B-ECD Fc fusion protein (R&D
460 systems). Phage particles fused with Fabs were incubated with an unrelated protein (e.g.
461 streptavidin) immobilized on a solid surface and allowed to bind in a step termed
462 counterselection to remove unwanted phage-Fabs prior to incubation against target. After
463 washing away unbound phage-Fab, phage were eluted from the target and amplified
464 overnight for subsequent rounds. After 5 rounds of this process individual clones from
465 rounds 3-5 were grown in 96-well format and tested by ELISA for their ability to bind
466 antigen specifically. We selected several unique and different positive Fab over 5 rounds
467 of selection, which were subcloned before antibody production (Proteogenix,
468 Schiltigheim, France).

469 ***Surface Plasmon Resonance***

470 Binding of anti-Unc5B antibodies to Human or Rat Unc5B was performed using a
471 Biacore™ 8K (Proteogenix, Schiltigheim, France). Human or Rat Unc5B-ECD-Fc (R&D
472 Systems) were immobilized on a CM5 sensor chip. Each antibody was diluted to gradient
473 concentrations (50nM, 25nM, 12.5nM, 6.25nM, 3.125nM) and flow through CM5 chip. The
474 kinetic parameter was calculated using Bia-evaluation analysis software.

475

476 ***Intravenous injection of antibodies, fluorescent tracer and***
477 ***nanobodies.***

478 CTRL Ab, anti-Unc5B-2 and -3 were injected intravenously into the lateral tail-vein of 8
479 weeks old adult mice at a concentration of 10mg of antibodies/kg of mice and left to
480 circulate from 1h to 24h depending on the experiment. All fluorescent tracers were
481 injected intravenously into the lateral tail vein of 8 weeks old adult mice and left to circulate
482 for 30min. Lysine-fixable Cadaverine conjugated to Alexa Fluor-555 (Invitrogen) was
483 injected at a concentration of 100ug Cadaverine/20g of mice. Lysine-fixable 10, 40 or 70
484 kDa dextran conjugated to tetramethylrhodamine (Invitrogen) were injected at a
485 concentration of 250ug dextran/20g of mice. Nanobodies (Alexa Fluor-488 coupled anti-
486 mouse nanobodies, Abnova) were injected at a concentration of 60ug nanobodies/20g of
487 mice and left to circulate for 30min. For postnatal experiment, cadaverine was injected
488 intraperitoneally into the P5 neonates at a concentration of 250ug cadaverine/20g of pups
489 and left to circulates 2h

490

491 ***Fluorescent tracer and nanobodies extravasation quantification***

492 To assess tracer leak, animals were perfused in the left ventricle with PBS. Brains (and
493 other organs) were then collected, and their weight measured. Next, brains (and other
494 organs) were incubated in formamide (Sigma-Aldrich, F7503) at 56°C for 48hours. Dye
495 fluorescence was then measured using a spectrophotometer at the adequate emission
496 and excitation wavelength. Dye extravasation from Unc5B^{fl/fl}, Unc5BiECko, WT treated
497 with CTRL Ab and anti-Unc5B-2 were performed at the Yale Cardiovascular Research
498 Center (New Haven, CT, USA) on a BioTek synergy2 spectrophotometer. Dye

499 extravasation from WT treated with CTRL IgG2b and anti-Unc5B-3 were performed at the
500 Paris Cardiovascular Research Center (Paris, France) on a Flexstation3
501 spectrophotometer. All results were normalized to the corresponding brain weight and
502 reported to a standard made of known concentrations of dye diluted in formamide. Results
503 are shown as ng of dye per mg of corresponding organ or tissue.

504

505 *BDNF extravasation quantification*

506 To assess BDNF leak, 1 hour after antibody injection, 50 µg of Human BDNF diluted in
507 saline was injected intravenously into the lateral tail vein in adult mice and left to circulate
508 for 30min. After sampling whole blood in EDTA-coated tubes, animals were perfused in
509 the left ventricle with saline. Brains were then collected, and their weight measured. Blood
510 was centrifuged at 1,000g for 15 minutes at 4°C, and plasma was then stored at -20°C
511 until use. Dissected brains were frozen in liquid nitrogen. They were lysed in RIPA buffer
512 (Thermo Fisher) supplemented with protease and phosphatase inhibitor cocktails (Roche,
513 11836170001 and 4906845001) with increasing needle gauges and sonicated (3 times
514 of 3 minutes each). All protein lysates were then centrifuged 15min at 14,000g at 4°C and
515 supernatants were isolated.

516 BDNF concentration in the plasma and brain lysates were quantified using a DuoSet
517 BDNF ELISA Kit (R&D Systems, DY248) according to manufacturer instructions. Results
518 were normalized to the corresponding brain weight. Results are shown as ng of
519 nanobodies per mg of brain tissue.

520

521 *MRI*

522 Magnetic resonance imaging (MRI) was performed in mice under isoflurane anesthesia
523 (2% in air) in a 4.7 T magnetic resonance scanner (Bruker BioSpec 47/40USR). Brain
524 images were obtained using a Spin-Echo (SE) T1 weighted sequence (TE/TR: 15/250
525 ms; matrix: 128x128; slice thickness: 1 mm; with no gap; 12 averages) in the axial and
526 coronal planes after intravenous injections of 100 µL gadoteric acid (0.1 mmol/mL).
527 Imaging was repeated every hour during the first 4 hours and at 24 hours after antibody
528 injection.

529 *Two photon Live imaging*

530 Craniotomy was performed by drilling a 5-mm circle between lambdoid, sagittal, and
531 coronal sutures of the skull on ketamine/xylazine anesthetized ROSAmT/mG mice. After
532 skull removal, the cortex was sealed with a glass coverslip cemented on top of the mouse
533 skull. Live imaging was done 2 weeks later. For multiphoton excitation of endogenous
534 fluorophores and injected dyes, we used a Leica SP8 DIVE in vivo imaging system
535 equipped with 4tune spectral external hybrid detectors and an InSightX3 laser
536 (SpectraPhysics). The microscope was equipped with in house designed mouse holding
537 platform for intravital imaging (stereotactic frame, Narishige; gas anesthesia and body
538 temperature monitoring/control, Minerve). Mice were injected intravenously with 10mg/kg
539 of UNC5B blocking or control antibodies and 1 hour later with dextran and/or Hoechst,
540 followed by imaging every five minutes over 30 to 90 minutes.

541

542 *Confocal microscopy*

543 Confocal images were acquired on a laser scanning fluorescence microscope (Leica SP8
544 and Zeiss LSM800) using the appropriate software (LASX or ZEN system). 10X, 20X and
545 63X oil immersion objectives were used for acquisition using selective laser excitation
546 (405, 488, 547, or 647 nm).

547

548 *Statistical analysis*

549 All *in vivo* experiments were done on littermates with similar body weight per condition
550 and reproduced on at least 3 different litters. Statistical analysis was performed using
551 GraphPad Prism 8 software. Mann-Whitney U test was performed for statistical analysis
552 on two groups. ANOVA followed by Bonferroni's multiple comparisons test was performed
553 for statistical analysis between 3 or more groups.

554

555

556

557

558

559 References

560 1 Zhao, Z., Nelson, A. R., Betsholtz, C. & Zlokovic, B. V. Establishment and Dysfunction of the
561 Blood-Brain Barrier. *Cell* **163**, 1064-1078, doi:10.1016/j.cell.2015.10.067 (2015).

562 2 Obermeier, B., Daneman, R. & Ransohoff, R. M. Development, maintenance and
563 disruption of the blood-brain barrier. *Nat Med* **19**, 1584-1596, doi:10.1038/nm.3407
564 (2013).

565 3 Zhou, Y. & Nathans, J. Gpr124 controls CNS angiogenesis and blood-brain barrier integrity
566 by promoting ligand-specific canonical wnt signaling. *Dev Cell* **31**, 248-256,
567 doi:10.1016/j.devcel.2014.08.018 (2014).

568 4 Eubelen, M. *et al.* A molecular mechanism for Wnt ligand-specific signaling. *Science* **361**,
569 doi:10.1126/science.aat1178 (2018).

570 5 Cho, C., Smallwood, P. M. & Nathans, J. Reck and Gpr124 Are Essential Receptor Cofactors
571 for Wnt7a/Wnt7b-Specific Signaling in Mammalian CNS Angiogenesis and Blood-Brain
572 Barrier Regulation. *Neuron* **95**, 1221-1225, doi:10.1016/j.neuron.2017.08.032 (2017).

573 6 Clevers, H. Wnt/beta-catenin signaling in development and disease. *Cell* **127**, 469-480,
574 doi:10.1016/j.cell.2006.10.018 (2006).

575 7 Liebner, S. *et al.* Wnt/beta-catenin signaling controls development of the blood-brain
576 barrier. *J Cell Biol* **183**, 409-417, doi:10.1083/jcb.200806024 (2008).

577 8 Daneman, R. *et al.* Wnt/beta-catenin signaling is required for CNS, but not non-CNS,
578 angiogenesis. *Proc Natl Acad Sci U S A* **106**, 641-646, doi:10.1073/pnas.0805165106
579 (2009).

580 9 Zhou, Y. *et al.* Canonical WNT signaling components in vascular development and barrier
581 formation. *J Clin Invest* **124**, 3825-3846, doi:10.1172/JCI76431 (2014).

582 10 Leonardo, E. D. *et al.* Vertebrate homologues of *C. elegans* UNC-5 are candidate netrin
583 receptors. *Nature* **386**, 833-838, doi:10.1038/386833a0 (1997).

584 11 Larrivee, B. *et al.* Activation of the UNC5B receptor by Netrin-1 inhibits sprouting
585 angiogenesis. *Genes Dev* **21**, 2433-2447, doi:10.1101/gad.437807 (2007).

586 12 Koch, A. W. *et al.* Robo4 maintains vessel integrity and inhibits angiogenesis by interacting
587 with UNC5B. *Dev Cell* **20**, 33-46, doi:10.1016/j.devcel.2010.12.001 (2011).

588 13 Zhang, F. *et al.* The Robo4 cytoplasmic domain is dispensable for vascular permeability
589 and neovascularization. *Nat Commun* **7**, 13517, doi:10.1038/ncomms13517 (2016).

590 14 Tai-Nagara, I. *et al.* Placental labyrinth formation in mice requires endothelial
591 FLRT2/UNC5B signaling. *Development* **144**, 2392-2401, doi:10.1242/dev.149757 (2017).

592 15 Yamagishi, S. *et al.* FLRT2 and FLRT3 act as repulsive guidance cues for Unc5-positive
593 neurons. *EMBO J* **30**, 2920-2933, doi:10.1038/emboj.2011.189 (2011).

594 16 Lu, X. *et al.* The netrin receptor UNC5B mediates guidance events controlling
595 morphogenesis of the vascular system. *Nature* **432**, 179-186, doi:10.1038/nature03080
596 (2004).

597 17 Wang, Y. *et al.* Ephrin-B2 controls VEGF-induced angiogenesis and lymphangiogenesis.
598 *Nature* **465**, 483-486, doi:10.1038/nature09002 (2010).

599 18 Munji, R. N. *et al.* Profiling the mouse brain endothelial transcriptome in health and
600 disease models reveals a core blood-brain barrier dysfunction module. *Nat Neurosci* **22**,
601 1892-1902, doi:10.1038/s41593-019-0497-x (2019).

602 19 Armulik, A. *et al.* Pericytes regulate the blood-brain barrier. *Nature* **468**, 557-561, doi:10.1038/nature09522 (2010).

603 20 Daneman, R., Zhou, L., Kebede, A. A. & Barres, B. A. Pericytes are required for blood-brain barrier integrity during embryogenesis. *Nature* **468**, 562-566, doi:10.1038/nature09513 (2010).

604 21 Cuervo, H. *et al.* PDGFRbeta-P2A-CreER(T2) mice: a genetic tool to target pericytes in angiogenesis. *Angiogenesis* **20**, 655-662, doi:10.1007/s10456-017-9570-9 (2017).

605 22 Zonta, M. *et al.* Neuron-to-astrocyte signaling is central to the dynamic control of brain microcirculation. *Nat Neurosci* **6**, 43-50, doi:10.1038/nn980 (2003).

606 23 Bauer, H. & Traweger, A. Tight Junctions of the Blood-Brain Barrier - A Molecular Gatekeeper. *CNS Neurol Disord Drug Targets* **15**, 1016-1029 (2016).

607 24 Luissint, A. C., Artus, C., Glacial, F., Ganeshamoorthy, K. & Couraud, P. O. Tight junctions at the blood brain barrier: physiological architecture and disease-associated dysregulation. *Fluids Barriers CNS* **9**, 23, doi:10.1186/2045-8118-9-23 (2012).

608 25 Niehrs, C. & Shen, J. Regulation of Lrp6 phosphorylation. *Cell Mol Life Sci* **67**, 2551-2562, doi:10.1007/s00018-010-0329-3 (2010).

609 26 Mao, B. *et al.* LDL-receptor-related protein 6 is a receptor for Dickkopf proteins. *Nature* **411**, 321-325, doi:10.1038/35077108 (2001).

610 27 Llambi, F., Causeret, F., Bloch-Gallego, E. & Mehlen, P. Netrin-1 acts as a survival factor via its receptors UNC5H and DCC. *EMBO J* **20**, 2715-2722, doi:10.1093/emboj/20.11.2715 (2001).

611 28 Wang, R. *et al.* Autoinhibition of UNC5b revealed by the cytoplasmic domain structure of the receptor. *Mol Cell* **33**, 692-703, doi:10.1016/j.molcel.2009.02.016 (2009).

612 29 Brault, V. *et al.* Inactivation of the beta-catenin gene by Wnt1-Cre-mediated deletion results in dramatic brain malformation and failure of craniofacial development. *Development* **128**, 1253-1264 (2001).

613 30 Harada, N. *et al.* Intestinal polyposis in mice with a dominant stable mutation of the beta-catenin gene. *EMBO J* **18**, 5931-5942, doi:10.1093/emboj/18.21.5931 (1999).

614 31 Taddei, A. *et al.* Endothelial adherens junctions control tight junctions by VE-cadherin-mediated upregulation of claudin-5. *Nat Cell Biol* **10**, 923-934, doi:10.1038/ncb1752 (2008).

615 32 Li, X. *et al.* VEGFR2 pY949 signalling regulates adherens junction integrity and metastatic spread. *Nat Commun* **7**, 11017, doi:10.1038/ncomms11017 (2016).

616 33 Knowland, D. *et al.* Stepwise recruitment of transcellular and paracellular pathways underlies blood-brain barrier breakdown in stroke. *Neuron* **82**, 603-617, doi:10.1016/j.neuron.2014.03.003 (2014).

617 34 Vanlandewijck, M. *et al.* A molecular atlas of cell types and zonation in the brain vasculature. *Nature* **554**, 475-480, doi:10.1038/nature25739 (2018).

618 35 Podjaski, C. *et al.* Netrin 1 regulates blood-brain barrier function and neuroinflammation. *Brain* **138**, 1598-1612, doi:10.1093/brain/awv092 (2015).

619 36 Yao, L. L. *et al.* Astrocytic neogenin/netrin-1 pathway promotes blood vessel homeostasis and function in mouse cortex. *J Clin Invest* **130**, 6490-6509, doi:10.1172/JCI132372 (2020).

644 37 Wang, Y. *et al.* Interplay of the Norrin and Wnt7a/Wnt7b signaling systems in blood-brain
645 barrier and blood-retina barrier development and maintenance. *Proc Natl Acad Sci U S A*
646 **115**, E11827-E11836, doi:10.1073/pnas.1813217115 (2018).

647 38 Huyghe, A. *et al.* Netrin-1 promotes naive pluripotency through Neo1 and Unc5b co-
648 regulation of Wnt and MAPK signalling. *Nat Cell Biol* **22**, 389-400, doi:10.1038/s41556-
649 020-0483-2 (2020).

650 39 Yang, J. M. *et al.* Dll4 Suppresses Transcytosis for Arterial Blood-Retinal Barrier
651 Homeostasis. *Circ Res* **126**, 767-783, doi:10.1161/CIRCRESAHA.119.316476 (2020).

652 40 Wang, Y. *et al.* Norrin/Frizzled4 signaling in retinal vascular development and blood brain
653 barrier plasticity. *Cell* **151**, 1332-1344, doi:10.1016/j.cell.2012.10.042 (2012).

654 41 Idbaih, A. *et al.* Safety and Feasibility of Repeated and Transient Blood-Brain Barrier
655 Disruption by Pulsed Ultrasound in Patients with Recurrent Glioblastoma. *Clin Cancer Res*
656 **25**, 3793-3801, doi:10.1158/1078-0432.CCR-18-3643 (2019).

657 42 Carpentier, A. *et al.* Clinical trial of blood-brain barrier disruption by pulsed ultrasound.
658 *Sci Transl Med* **8**, 343re342, doi:10.1126/scitranslmed.aaf6086 (2016).

659 43 Sheikov, N., McDannold, N., Vakhodtseva, N., Jolesz, F. & Hynynen, K. Cellular
660 mechanisms of the blood-brain barrier opening induced by ultrasound in presence of
661 microbubbles. *Ultrasound Med Biol* **30**, 979-989, doi:10.1016/j.ultrasmedbio.2004.04.010
662 (2004).

663 44 Aryal, M., Arvanitis, C. D., Alexander, P. M. & McDannold, N. Ultrasound-mediated blood-
664 brain barrier disruption for targeted drug delivery in the central nervous system. *Adv Drug
665 Deliv Rev* **72**, 94-109, doi:10.1016/j.addr.2014.01.008 (2014).

666 45 Hadi, T. *et al.* Macrophage-derived netrin-1 promotes abdominal aortic aneurysm
667 formation by activating MMP3 in vascular smooth muscle cells. *Nat Commun* **9**, 5022,
668 doi:10.1038/s41467-018-07495-1 (2018).

669 46 Persson, H. *et al.* CDR-H3 diversity is not required for antigen recognition by synthetic
670 antibodies. *J Mol Biol* **425**, 803-811, doi:10.1016/j.jmb.2012.11.037 (2013).

671

672

673 Acknowledgements

674 This project has received funding from the NIH (1R01HL149343-01, 1R01DK120373-
675 01A1 to AE, 5R01NS35900 to SLA), the Leducq Foundation (TNE ATTRACT, AE, LCW),
676 INSERM and the European Research Council (ERC) (grant agreement No. 834161 to
677 AE). KB was supported by a fellowship from the AHA (18POST34070109). We thank Max
678 Thomas for technical assistance. SLA is an investigator of the Howard Hughes Medical
679 Institute.

680

681

682 **Data availability**

683 All data generated are included in this article (main or supplementary information files).

684 Additional information can be obtained from the corresponding author upon reasonable

685 request.

686

687 **Competing interests declaration**

688 A.E., K.B., L.G. and L.P-F. are inventors on two patent application submitted by Yale

689 University that covers the use and generation process of Unc5B blocking antibodies, and

690 their application.

Figure 1

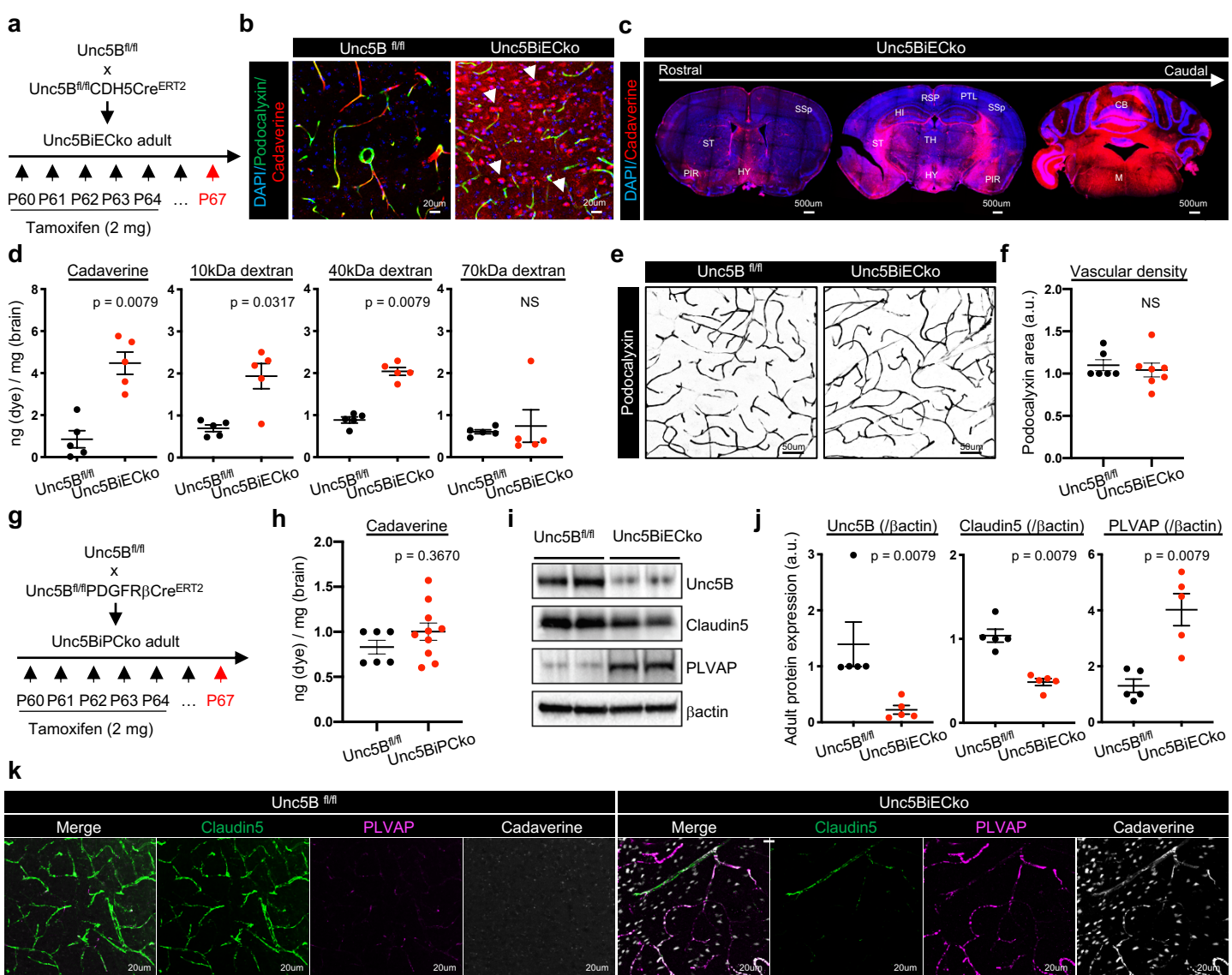


Figure 1: Unc5B controls BBB integrity.

(a) *Unc5B* gene deletion strategy using tamoxifen (TAM) injection in adult mice. (b,c) Immunofluorescence staining with the indicated markers and confocal imaging 7 days after TAM injection and 30 min after i.v cadaverine injection. (d) Quantification of brain dye content 7 days after TAM injection and 30min after i.v. injection of dyes with increasing MW (n = 5 mice/group). (e,f) Adult *Unc5B^{fl/fl}* and *Unc5BiECko* brain vessel immunofluorescence using the luminal marker podocalyxin and quantification of vascular density. (g,h) *Unc5B^{fl/fl}* was crossed with *PDGFR β Cre^{ERT2}* and BBB permeability was assessed 7 days after the last TAM injection and 30 min after cadaverine injection i.v. (n > 6 mice/group). (i,j) Western blot and quantification of adult *Unc5B^{fl/fl}* and *Unc5BiECko* brain protein extracts, n = 5 animals/group. (k) Immunofluorescence staining with the indicated antibodies and confocal imaging of adult *Unc5B^{fl/fl}* and *Unc5BiECko* piriform cortex 7 days after TAM injection and 30 min after i.v cadaverine injection. All data are shown as mean+/-SEM. NS: non-significant, PIR: Piriform cortex, RSP: Retrosplenial cortex, HI: Hippocampus, HY: Hypothalamus, TH: Thalamus, ST: Striatum, PTL: Posterior parietal association areas, SSp: Primary somatosensory cortex, CB: Cerebellum, M: Medulla. Mann-Whitney U test was performed for statistical analysis.

Figure 2

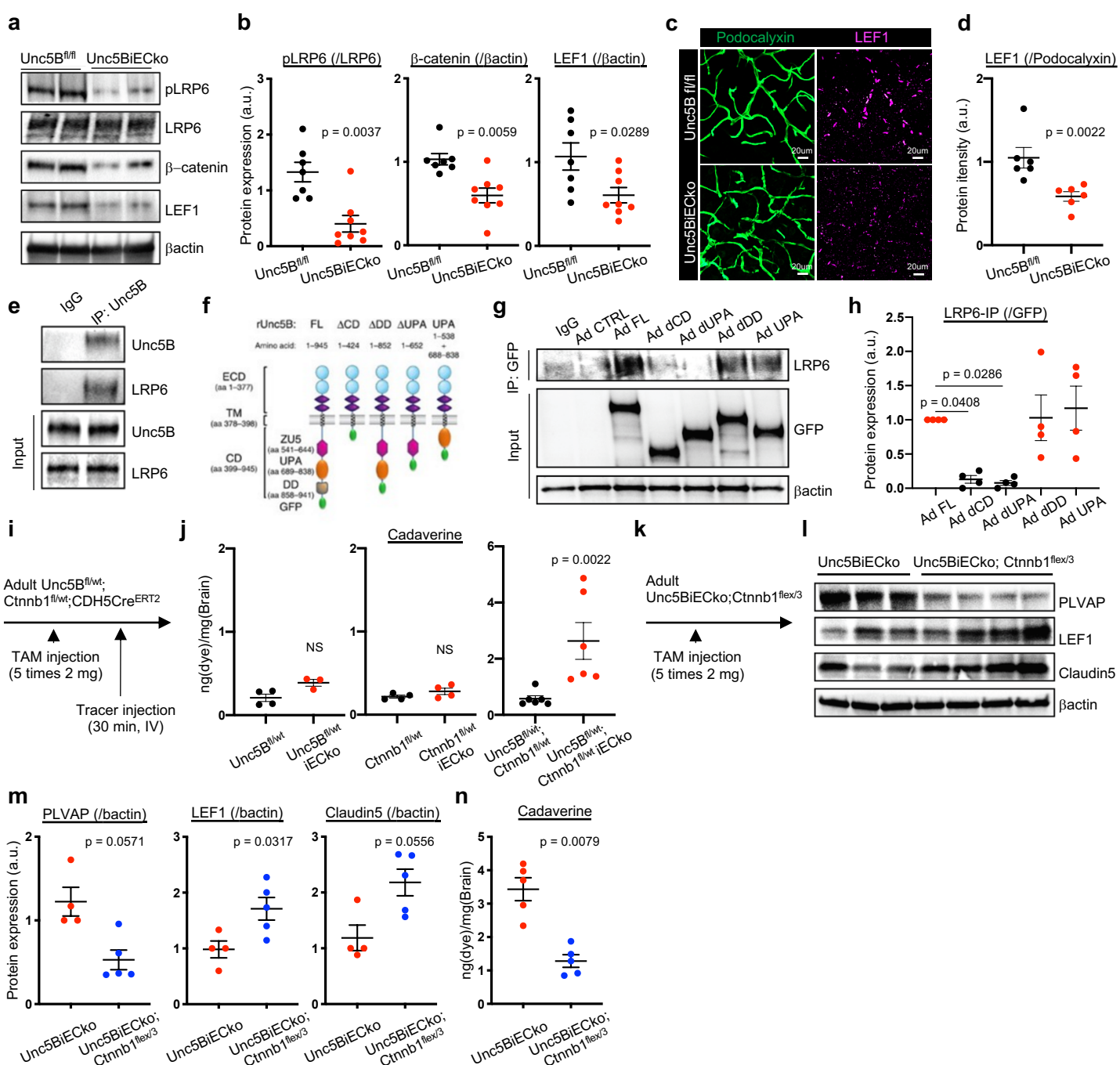


Figure 2: Unc5B regulates the BBB via Wnt/β-catenin signaling.

(a,b) Western blot and quantification of Wnt signaling components in adult *Unc5B^{fl/fl}* and *Unc5BiECko* brain protein extracts, n > 7 mice per group. (c,d) Immunofluorescence and quantification of LEF1 staining on adult *Unc5B^{fl/fl}* and *Unc5BiECko* brain vibratome sections. (e) IgG control and Unc5B immunoprecipitation on cultured brain endothelial cells. (f) Unc5B GFP-adenovirus schematic. (g,h) IgG control or GFP immunoprecipitation in ECs infected with Unc5B constructs. (i,j) Quantification of brain cadaverine content in adult mice, 7 days after the last TAM injection and 30 min after i.v cadaverine injection. (k-m) Western blot and quantification of adult *Unc5BiECko* and *Unc5BiECko*; *Ctnnb1flex/3* brain protein extracts, n > 4 mice per group. (n) Quantification of brain cadaverine content in adult mice, 7 days after the last TAM injection and 30 min after i.v cadaverine injection. (n = 5 mice per group). All data are shown as mean+/- SEM. NS: non-significant. Mann-Whitney U test was performed for statistical analysis between two groups. ANOVA followed by Bonferroni's multiple comparisons test was performed for statistical analysis between multiple groups.

Figure 3

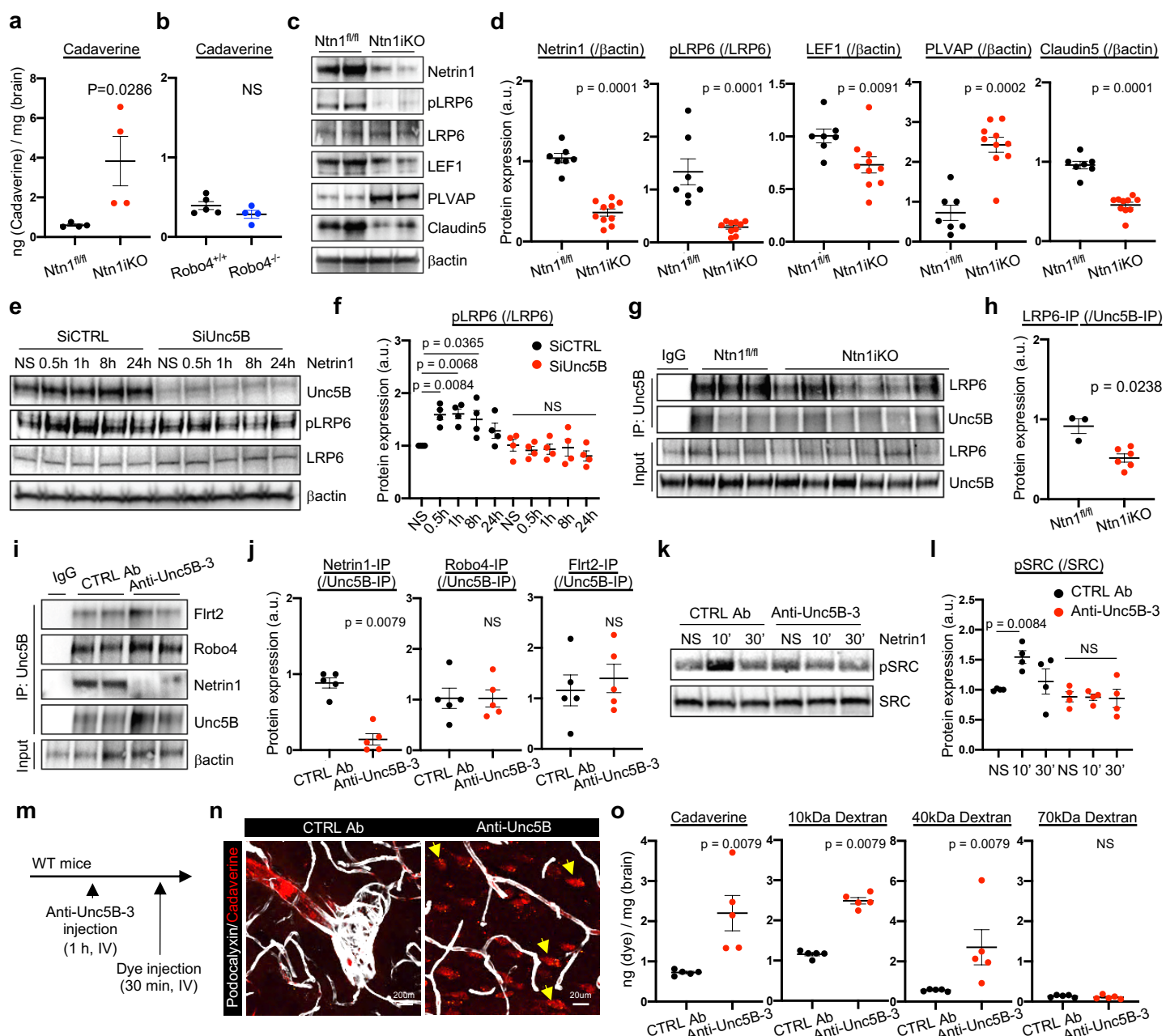


Figure 3: Netrin1 binding to Unc5B regulates Wnt/β-catenin signaling to maintain BBB integrity.

(a,b) Quantification of brain cadaverine content in adult mice, 7 days after the last TAM injection (a) and 30 min after i.v cadaverine injection (n = 4 mice/group). (c,d) Western blot and quantification of adult brain protein extracts from *Ntn1*^{f/f} and Ntn1iKO mice (n>7 mice per group). (e,f) Western blot and quantification of brain ECs treated with SiCTRL or SiUnc5B before Netrin1 treatment for the indicated times. (g,h) Unc5B immunoprecipitation of brain protein extracts and LRP6 western blot and quantification. (i,j) Unc5B immunoprecipitation of brain protein extracts from mice i.v injected with CTRL or anti-Unc5B-3 antibodies (1 h, 10 mg/kg) and western blot with antibodies recognizing the indicated ligands and quantification (n = 5 mice per group). (k,l) Western-blot and protein quantification of ECs treated with CTRL or anti-Unc5B-3 for 1h followed by Netrin1 stimulation (500 ng/ml) for 10 min or 30 min (n = 4). (m,n) BBB permeability was assessed by immunofluorescence on brain vibratome section from mice injected with CTRL or anti-Unc5B-3 antibodies i.v. (1 h, 10 mg/kg). (o) Quantification of brain dye content 30 min after injection of dyes with increasing MW and 1 h after CTRL or anti-Unc5B-3 i.v. injection (10 mg/kg). All data are shown as mean+/-SEM. NS: non-significant. Mann-Whitney U test was performed for statistical analysis between two groups. ANOVA followed by Bonferroni's multiple comparisons test was performed for statistical analysis between multiple groups.

Figure 4

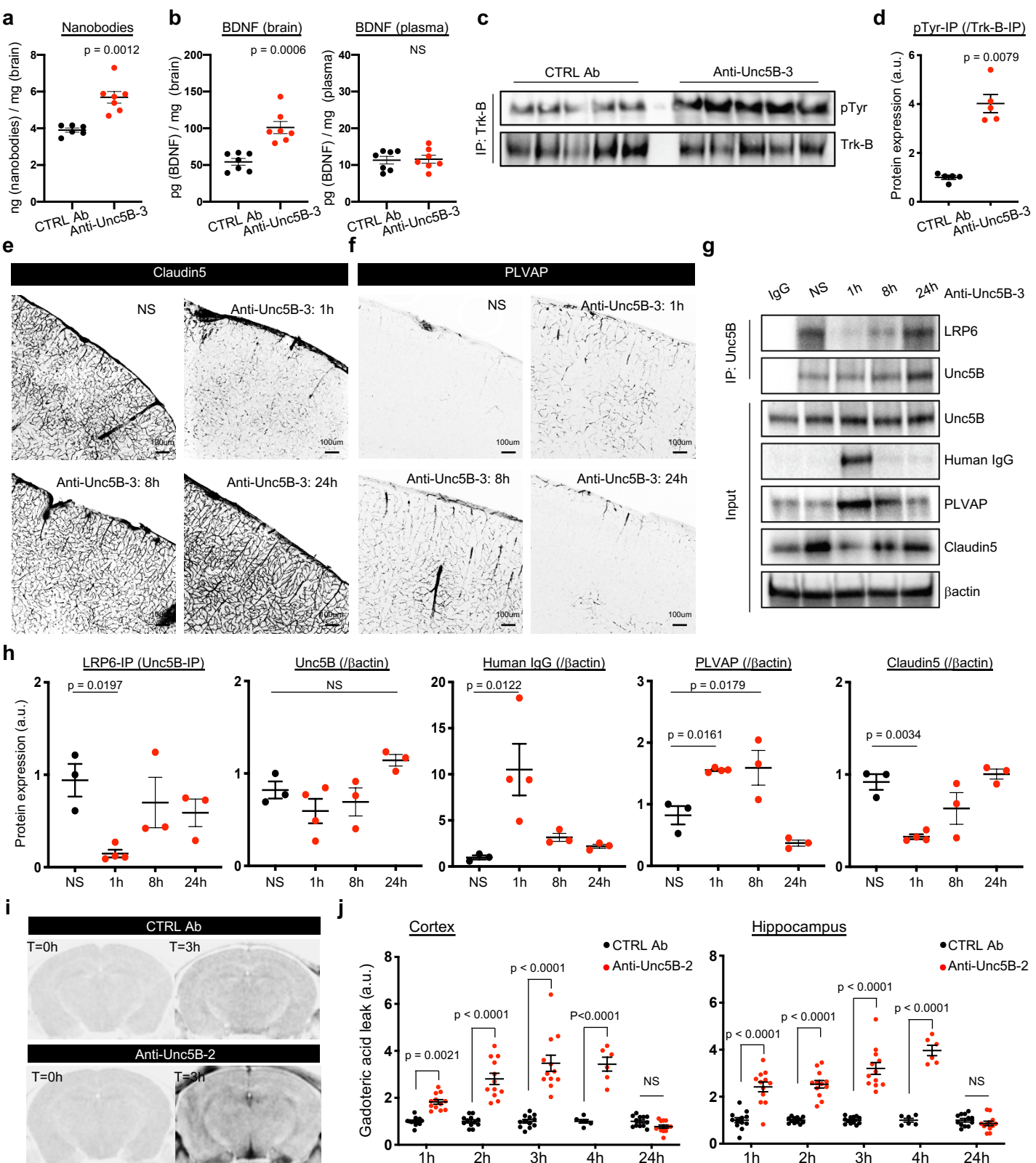
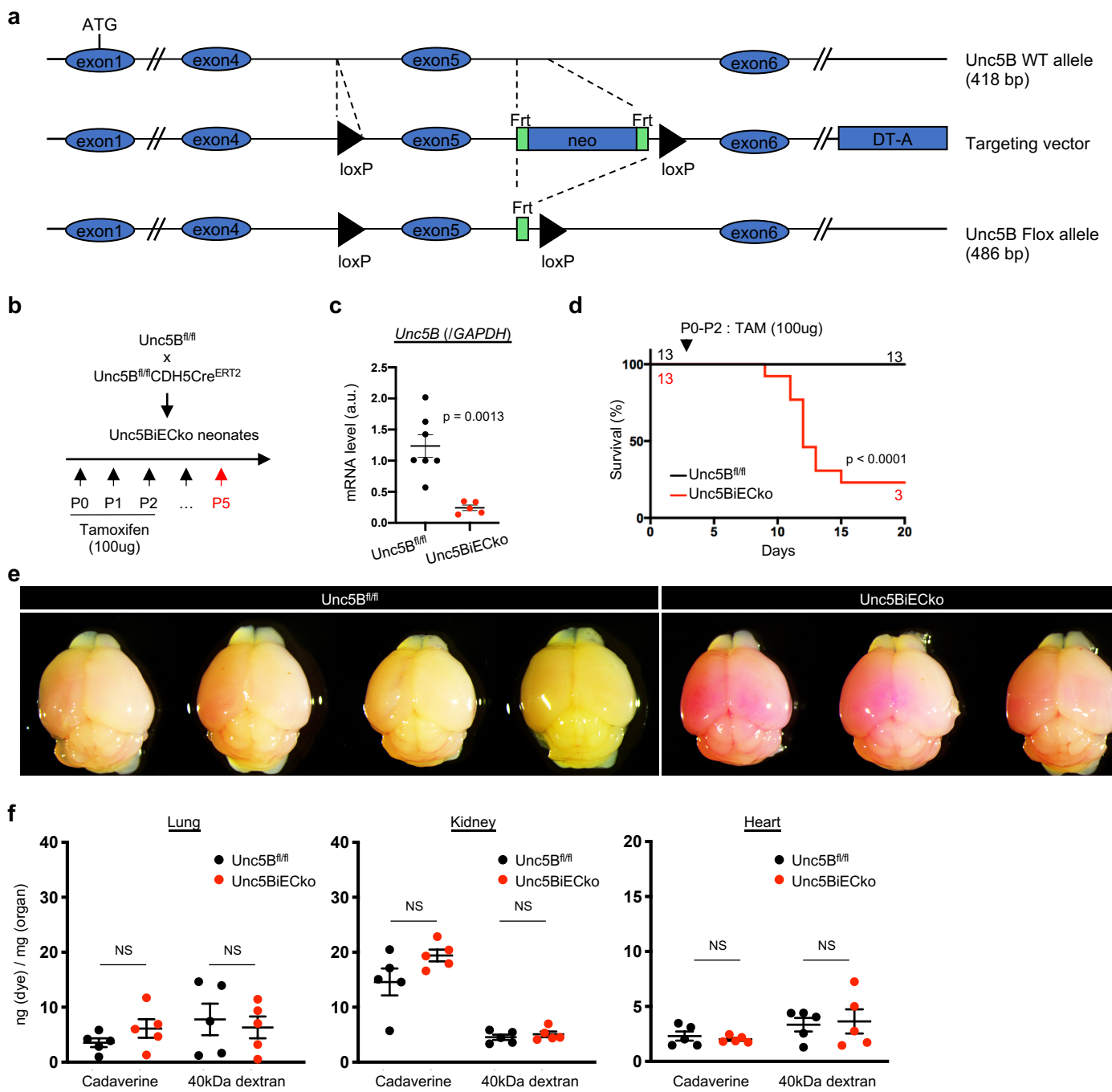


Figure 4: Reversible BBB opening by Unc5B-blocking antibodies.

(a) Quantification of brain nanobody content 1h after i.v CTRL or anti-Unc5B-3 injection (10 mg/kg) and 30min after i.v nanobody injection. (b) Quantification of brain and plasma BDNF concentration 1 h after i.v CTRL or anti-Unc5B-3 injection (10mg/kg) and 30m in after i.v BDNF injection. (c,d) Trk-B immunoprecipitation and anti-phospho-tyrosine western blot on brain protein extracts from mice injected with CTRL or anti-Unc5B-3 antibodies i.v. (1h, 10mg/kg) followed by BDNF injection for 30 min (n = 5 mice per group). (e,f) Immunofluorescence staining of Claudin5 and PLVAP on adult brain vibratome section from mice i.v. injected with anti-Unc5B-3 (10 mg/kg) for 1, h or 24 h. (g,h) Unc5B immunoprecipitation and quantification of brain protein extracts from mice injected with anti-Unc5B-3 i.v. (10 mg/kg) for 1, 8 or 24 h, n = 3/4 animals/group. (i,j) MRI analysis and quantification of gadolinium leakage after CTRL or anti-Unc5B-2 injection. Gadolinium was injected 1, 2, 3, 4 and 24 h after the antibodies. All data are shown as mean+/-SEM. NS: non-significant. Mann-Whitney U test was performed for statistical analysis between two groups. ANOVA followed by Bonferroni's multiple comparisons test was performed for statistical analysis between multiple groups.

Supp Fig. 1

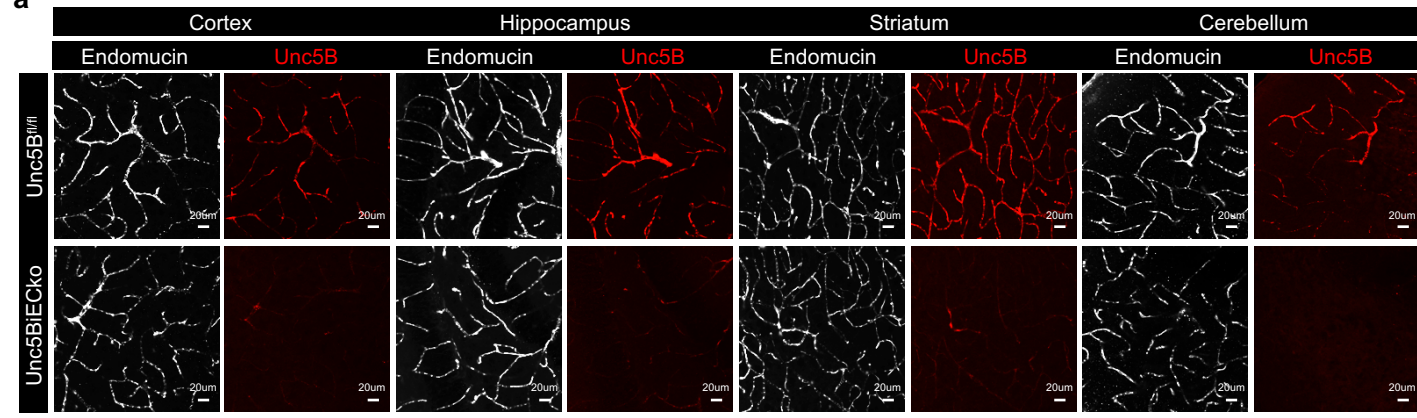


Supplemental Figure 1:

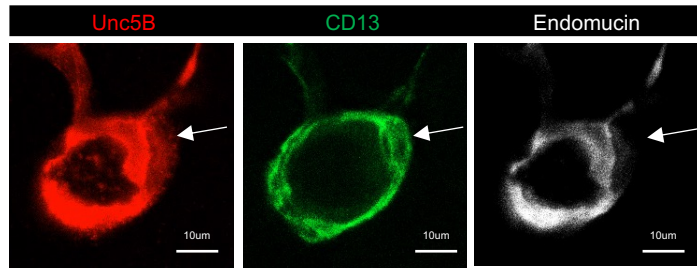
(a) Diagram illustrating generation of the *Unc5B* Flox allele. (b) *Unc5B* gene deletion strategy using tamoxifen (TAM) injection in postnatal mice. (c) qPCR analysis of *Unc5B* mRNA on isolated P5 mouse lung endothelial cells, n>5 mice/group. (d) Survival curve after neonatal *Unc5B* gene deletion (n = 13 mice per group). (e) Cadaverine leakage in P5 *Unc5B^{f/f}* and *Unc5BiECko* brains 2 h after intraperitoneal cadaverine injection. (f) Quantification of organ dye content in adult mice, 7 days after the last TAM injection and 30min after i.v injection of dyes with increasing MW (n = 5 mice per group). All data are shown as mean+/-SEM. NS: non-significant. Mann-Whitney U test was performed for statistical analysis between two groups.

Supp Fig. 2

a



b

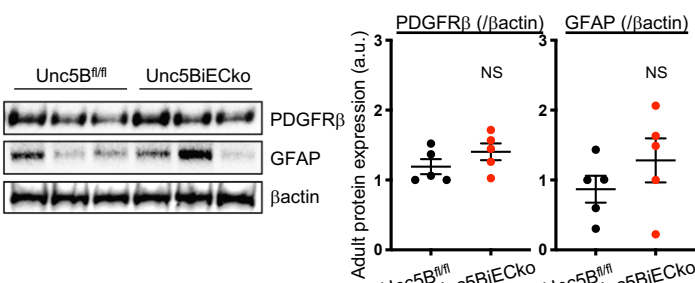


Supplemental Figure 2:

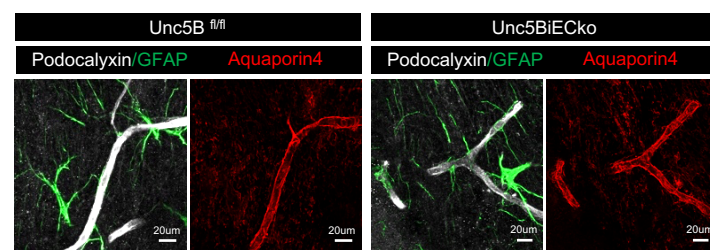
(a,b) Immunofluorescence staining with the indicated antibodies and confocal imaging of vibratome sections from several brain regions.

Supp Fig. 3

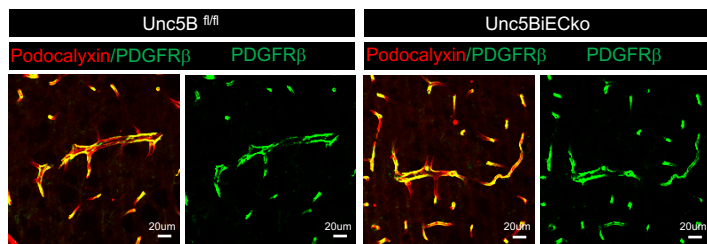
a



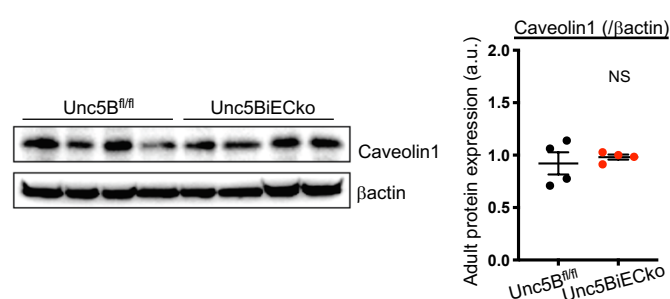
b



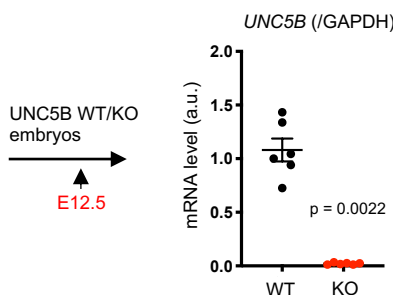
c



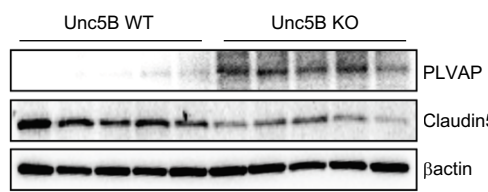
d



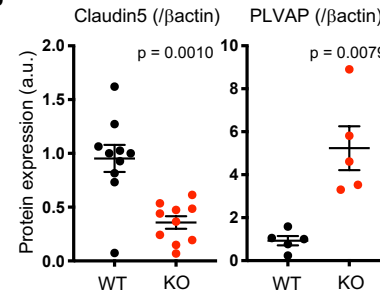
e



f



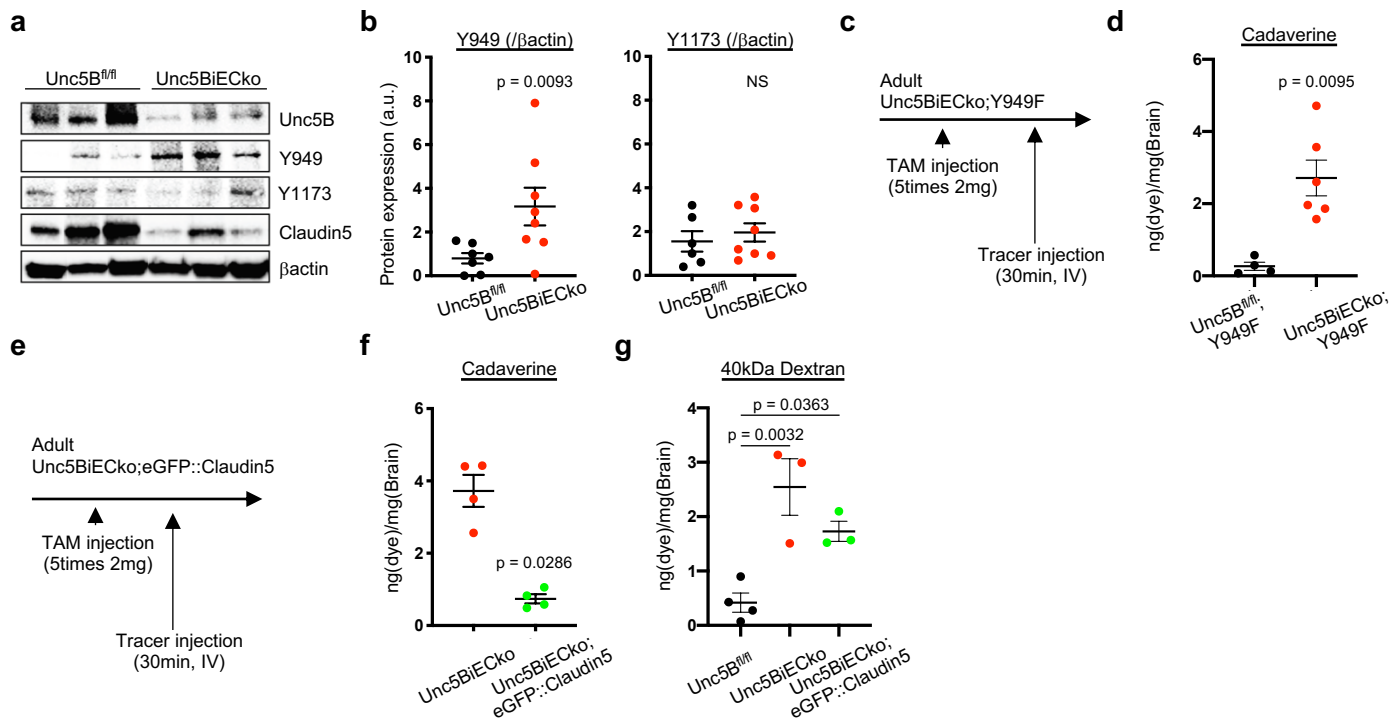
g



Supplemental Figure 3:

(a) Western blot and quantification of adult *Unc5B*^{fl/fl} and Unc5BiECko brain protein extracts (n=5 mice per group). (b,c) Immunofluorescence staining with the indicated antibodies and confocal imaging 7 days after TAM injection. (d) Western blot and quantification of adult *Unc5B*^{fl/fl} and Unc5BiECko brain protein extracts, n = 5 animals/group. (e) qPCR analysis on E12.5 brain mRNA extracts from *Unc5B* global KO mice, n = 6 embryos/group. (f,g) Western blot and quantification of E12.5 *Unc5B* WT and KO brain protein extracts (n>5 animals/group). All data are shown as mean+/-SEM. NS: non-significant, Mann-Whitney U test was performed for statistical analysis.

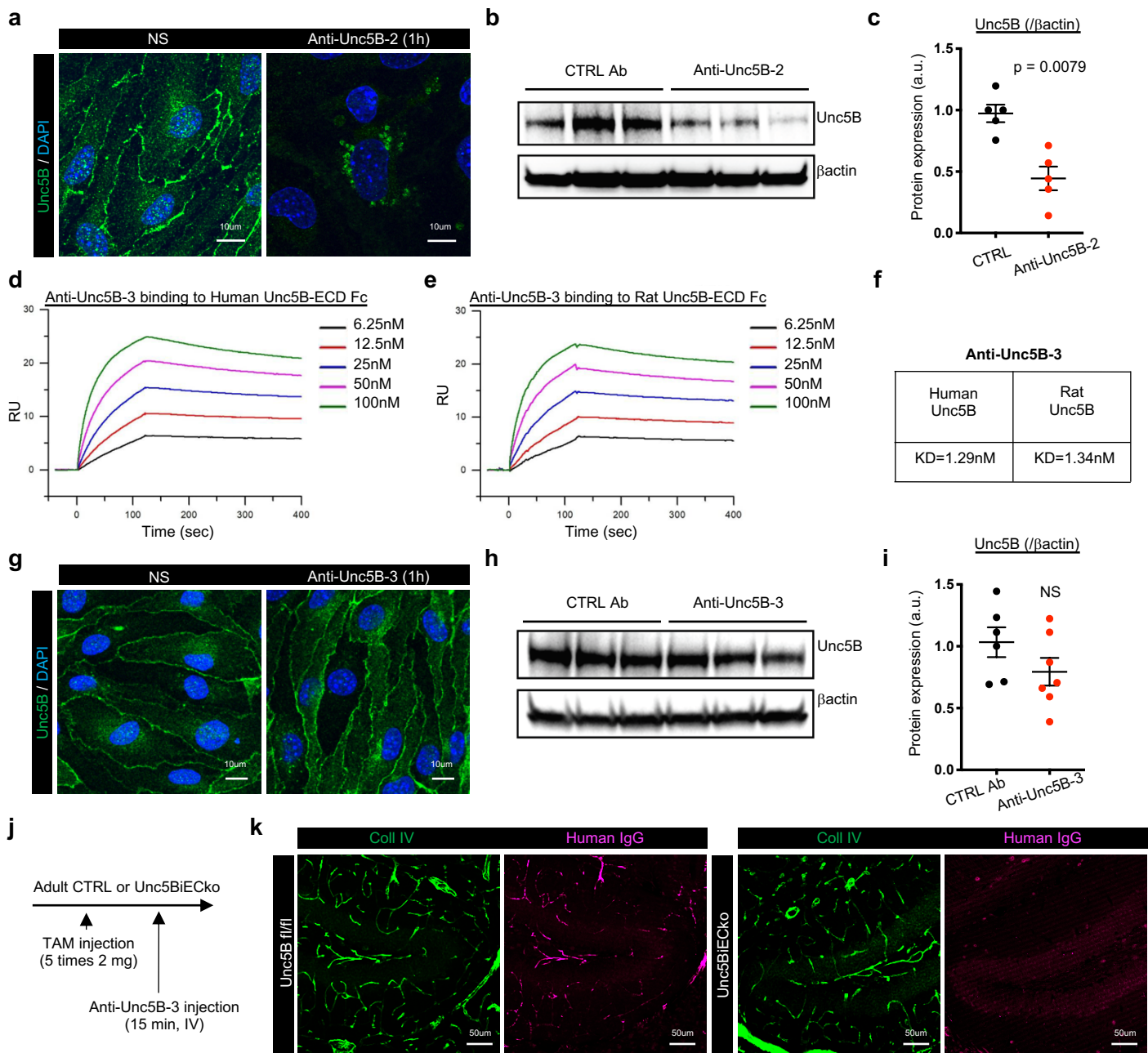
Supp Fig. 4



Supplemental Figure 4:

(a, b) Western blot and quantification of Vegfr2 signaling in adult *Unc5B^{fl/fl}* and *Unc5BiECKo* brain protein extracts, n > 7 mice per group. (c, d) Quantification of brain cadaverine content in adult mice, 7 days after TAM injection and 30 min after i.v. cadaverine injection (n > 4 mice per group). (e-g) Quantification of brain dye content in adult mice, 7 days after TAM injection and 30 min after i.v. cadaverine or 40kDa dextran injection (n > 3 mice per group). All data are shown as mean+/-SEM. NS: non-significant. Mann-Whitney U test was performed for statistical analysis between two groups. ANOVA followed by Bonferroni's multiple comparisons test was performed for statistical analysis between multiple groups.

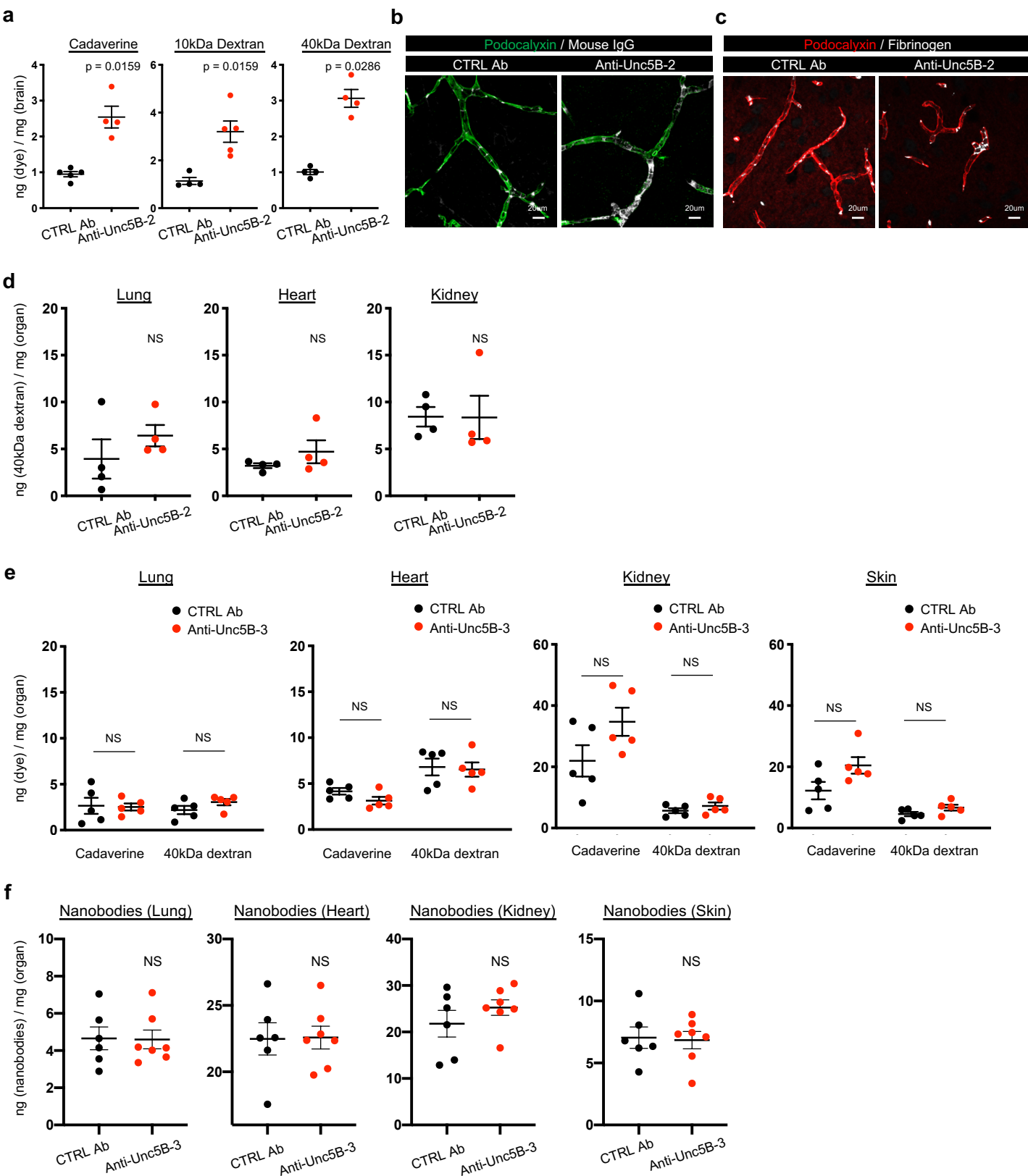
Supp Fig. 5



Supplemental Figure 5:

(a) Unc5B immunofluorescence detected with a commercial anti-Unc5B antibody and confocal imaging of confluent monolayers of mouse brain ECs (Bend3) treated or not with anti-Unc5B-2 for 1 h. (b,c) Western blot and quantification on brain protein extracts from mice i.v injected with CTRL or anti-Unc5B-2 antibodies (1 h, 10 mg/kg) (n = 5 mice per group). (d-f) Surface Plasmon Resonance measurements of anti-Unc5B-3 binding to human and rat Unc5B. (g) Unc5B immunofluorescence detected with a commercial anti-Unc5B antibody and confocal imaging of confluent monolayers of mouse brain ECs (Bend3) treated or not with anti-Unc5B-3 for 1 h. (h,i) Western-blot and quantification on brain protein extracts from mice i.v. injected with CTRL or anti-Unc5B-3 antibodies (1 h, 10 mg/kg) (n = 5 mice per group). (j,k) Anti-Unc5B-3 was i.v. injected in *Unc5B*^{fl/fl} or *Unc5BiEC*ko mice for 20min, mice were perfused and anti-Unc5B-3 binding was revealed by immunofluorescence on brain vibratome section using an anti-human IgG antibody. All data are shown as mean+/-SEM. NS: non-significant, Mann-Whitney U test was performed for statistical analysis.

Supp Fig. 6

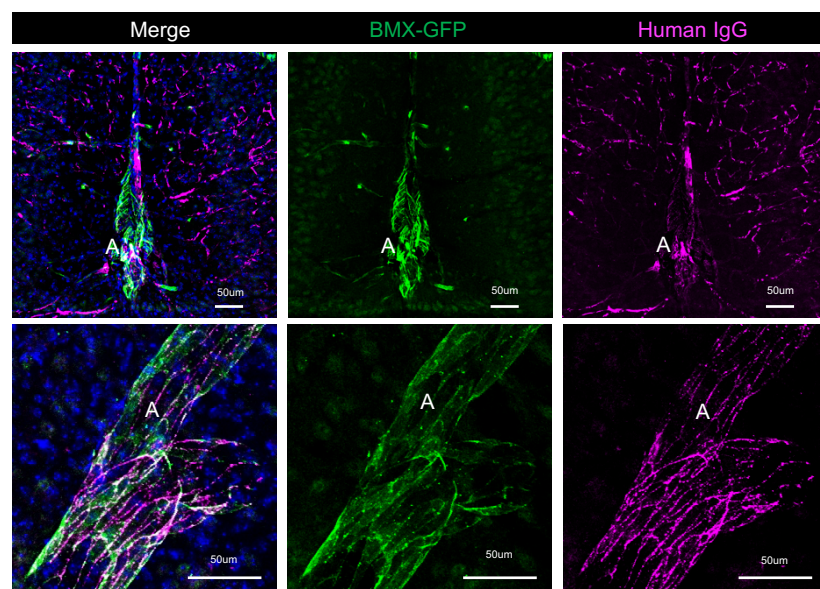


Supplemental Figure 6:

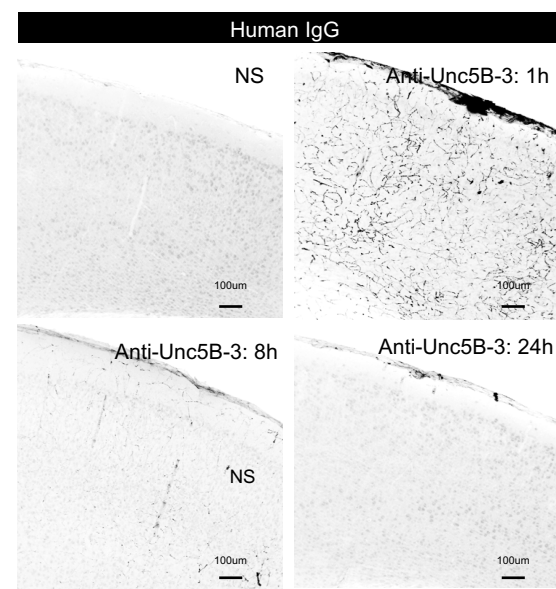
(a) Quantification of brain dye content 30min after injection of dyes with increasing MW and 1h after CTRL or anti-Unc5B-2 i.v. injection (10 mg/kg) (n > 4 mice per group). (b,c) Immunofluorescence of blood vessels (podocalyxin) and endogenous IgG and fibrinogen on brain vibratome sections 1 h after CTRL or anti-Unc5B-2 i.v. injection (10 mg/kg). (d,e) Quantification of organ dye content 1 h after i.v. CTRL or anti-Unc5B-2 or anti-Unc5B-3 injection (10 mg/kg) and 30min after i.v injection of dyes with increasing MW in adult mice (n > 4 mice per group). (f) Quantification of organ nanobody content 1 h after i.v CTRL or anti-Unc5B-3 injection (10 mg/kg) and 30 min after i.v nanobody injection (n = 5 mice per group). All data are shown as mean+/-SEM. NS: non-significant, Mann-Whitney U test was performed for statistical analysis.

Supp Fig. 7

a



b

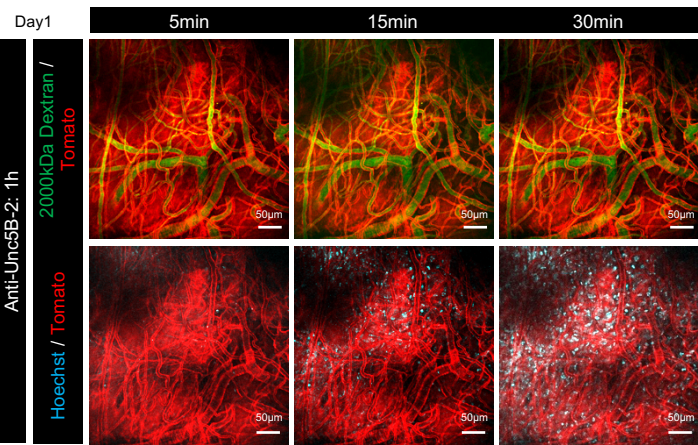


Supplemental Figure 7:

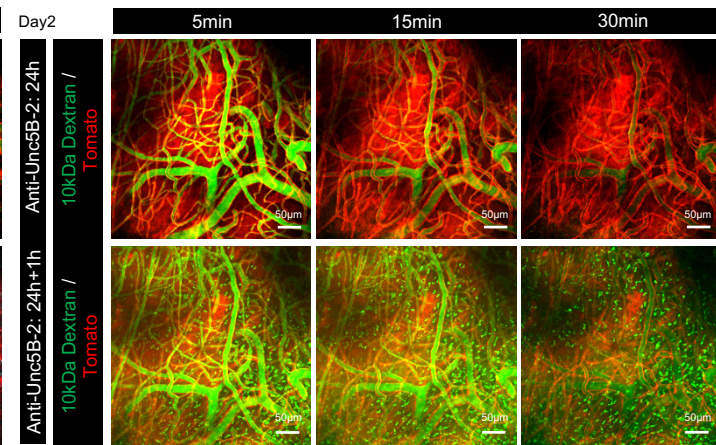
(a) TAM was injected for 5 days in *BMXCre^{ERT2}-mTmG* mice followed by anti-Unc5B-3 i.v. injection for 15 min. After cardiac perfusion, anti-Unc5B binding was revealed by immunofluorescence using anti-human IgG antibody followed by confocal imaging. (b) Immunofluorescence staining of anti-human IgG antibody on adult brain vibratome section from mice i.v. injected with anti-Unc5B-3 (10mg/kg) for 1, 8 or 24 h.

Supp Fig. 8

a



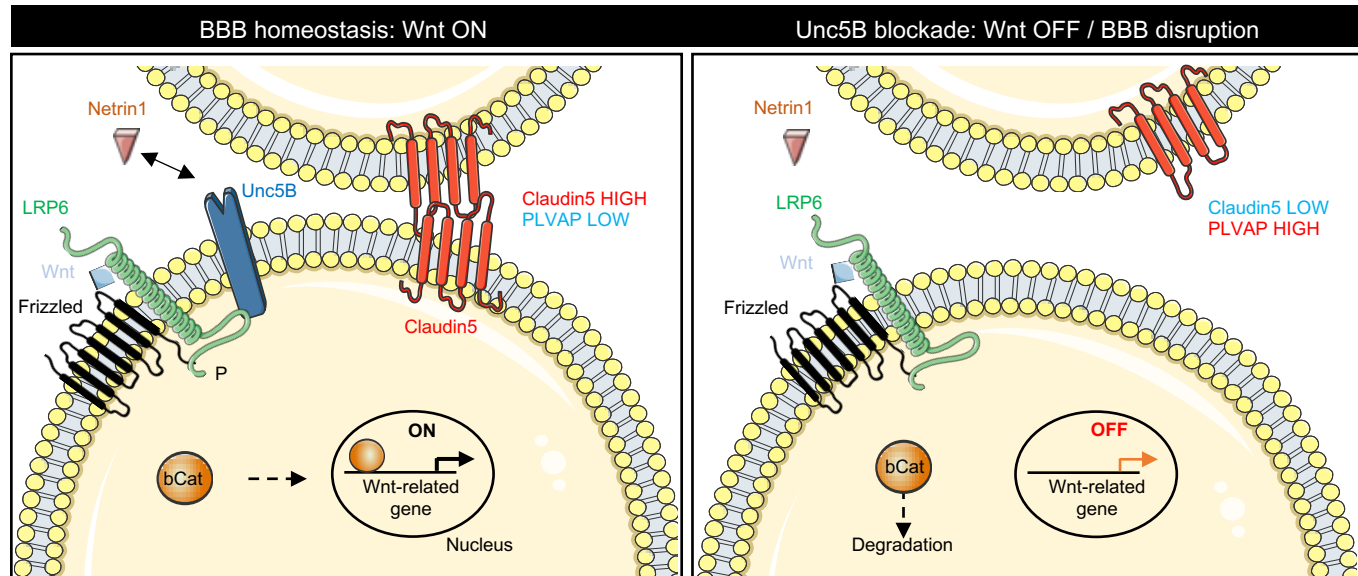
b



Supplemental Figure 8:

(a) Two-photon live imaging of *C57BL/6; ROSAmTmG* mice 1h after i.v. injection of anti-Unc5B-2 (1 h, 10 mg/kg) and 5, 15 or 30 min after i.v. injection of 2000kDa FITC-dextran and 560Da Hoechst. Note leakage of Hoechst 15 to 30min after i.v. injection while 2000kDa FITC-dextran outlined the brain vasculature. (b) Two-photon live imaging of mice that were treated with the anti-Unc5B-2 antibody 24 h earlier, 5, 15 and 30 min after i.v. injection of 10kDa FITC-dextran. Note the absence of BBB leakage. Next, mice received a second i.v. injection of anti-Unc5B-2 (10 mg/kg) for 1h followed by another i.v. injection of 10kDa FITC-dextran and two-photon live imaging revealed BBB leakage.

Supp Fig. 9



Supplemental Figure 9:

Netrin1 binding to endothelial Unc5B regulates Wnt/β-catenin signaling and BBB integrity.

In the absence of Netrin1-Unc5B signaling the Wnt/β-catenin signaling is disrupted which induced loss of Claudin5 along with increased PLVAP expression and BBB leakage.